
Masters Theses

Student Theses and Dissertations

Fall 2010

Full wave simulation of an electrostatic discharge generator discharging in air discharge mode into a product and quantify channel performance utilizing novel time domain convolution method

Dazhao Liu

Follow this and additional works at: https://scholarsmine.mst.edu/masters_theses



Part of the [Electrical and Computer Engineering Commons](#)

Department:

Recommended Citation

Liu, Dazhao, "Full wave simulation of an electrostatic discharge generator discharging in air discharge mode into a product and quantify channel performance utilizing novel time domain convolution method" (2010). *Masters Theses*. 6788.

https://scholarsmine.mst.edu/masters_theses/6788

This thesis is brought to you by Scholars' Mine, a service of the Missouri S&T Library and Learning Resources. This work is protected by U. S. Copyright Law. Unauthorized use including reproduction for redistribution requires the permission of the copyright holder. For more information, please contact scholarsmine@mst.edu.

FULL WAVE SIMULATION OF AN ELECTROSTATIC DISCHARGE GENERATOR
DISCHARGING IN AIR DISCHARGE MODE INTO A PRODUCT
AND
QUANTIFY CHANNEL PERFORMANCE UTILIZING NOVEL TIME DOMAIN
CONVOLUTION METHOD

by

DAZHAO LIU

A THESIS

Presented to the Faculty of the Graduate School of the
MISSOURI UNIVERSITY OF SCIENCE AND TECHNOLOGY

In Partial Fulfillment of the Requirements for the Degree

MASTER OF SCIENCE IN ELECTRICAL ENGINEERING

2010

Approved by

Dr. Jun Fan, Advisor
Dr. James L. Drewniak
Dr. David J. Pommerenke

© 2010

Dazhao Liu

All Rights Reserved

ABSTRACT

In the first section, it introduces a methodology to simulate the currents and fields during an air discharge ESD into a product by combining a linear description of the behavior of the DUT with a non-linear arc resistance equation. The most commonly used test standard IEC 61000-4-2 requires using contact mode discharges to metallic surfaces and air discharge mode to non-conducting surfaces. In contact mode, an Electrostatic Discharge (ESD) generator is a linear system. In air discharge mode, a highly non-linear arc is part of the current loop. This paper proposes a method that combines the linear ESD generator full wave model and the non-linear arc model to simulate currents and fields in air discharge mode. Measurements are presented comparing discharge currents and fields for two cases: ESD generator discharges into a ground plane and ESD generator discharges into a small product.

In the second section, it presents a novel time domain convolution based methodology to quantify channel performance by calculating difference waveform distortion penalty (dWDP). Instead of using frequency based methodology as indicated in the SFF-8431 standard, the pulse response can be used in convolution to obtain the channel output when a NRZ sequence is transmitted through a channel. However, the proposed method utilizing the step response can significantly reduce the convolution time.

ACKNOWLEDGMENTS

I would like to express my sincere gratitude to Dr. Jun Fan, my advisor, for his teaching, instruction, warm encouragement on my research work, financial support to my study and direction for this thesis during my pursuit of the Master's degree.

I would like to thank Dr. David Pommerenke, my advisor for my first year in Rolla, for his enlightening to my research motion and teaching me how to walk on water.

I would like to thank Dr. James Drewniak, my mentor during my transition time, the most difficult days when I got rid of my immaturity and irresponsibility, for giving me faith, trust, and encouragement.

I would like to thank Dr. Daryl Beetner, and Dr. Richard DuBroff, for their teaching in my courses, discussions related to my research and helpful suggestions on my thesis.

I would also like to express my thanks to all the other faculty members and students in the UMR/S&T EMC lab for their team work and help in my research and coursework. It has been my great pleasure to work with you!

Finally, I would like to thank my family for their love and my girlfriend Qian for her unconditional support during the past two years of my life.

TABLE OF CONTENTS

	Page
ABSTRACT	iii
ACKNOWLEDGMENTS	iv
LIST OF ILLUSTRATIONS	vii
LIST OF TABLES	ix
SECTION	
1. FULL WAVE SIMULATION OF AN ELECTROSTATIC DISCHARGE GENERATOR DISCHARGING IN AIR DISCHARGE MODE.....	1
1.1. INTRODUCTION	1
1.2. METHODOLOGY	2
1.3. CASE 1: ESD GENERATOR DISCHARGE TO A GROUND PLANE	6
1.3.1. Z11 Between the Tip of the ESD Generator and the Ground Plane.....	6
1.3.2. SPICE Simulation for the Discharge Current.....	8
1.3.3. Re-import of Currents into CST.....	9
1.3.4. Validation by Measurement Results.....	9
1.4. CASE 2: ESD GENERATOR DISCHARGE INTO A SMALL PRODUCT ..	11
1.4.1. Z11 Between the Tip of the ESD Generator and the Product	11
1.4.2. SPICE Simulation for the Discharge Current.....	14
1.4.3. Re-import of Currents into CST.....	15
1.4.4. Validation by Measurement Results.....	16
1.4.4.1 Measured discharge current	18
1.4.4.2 Measured magnetic field.....	21
1.5. DISCUSSION.....	22
1.6. CONCLUSION.....	24
2. CHANNEL PERFORMANCE CERTIFICATION UTILIZING NOVEL TIME DOMAIN CONVOLUTION METHODD.....	25
2.1. INTRODUCTION	25
2.2. TIME DOMAIN METHODOLOGY USING S-PARAMETERS	27
2.2.1. dWDP	28
2.2.1.1 Using step response.....	28

2.2.1.2	Get causal step response from S-parameters	29
2.2.1.3	Shift and add step response.....	39
2.2.2.	NEXT	41
2.2.2.1	Statistical estimation using pulse response	41
2.2.2.2	Get reasonable pulse response	47
2.2.2.3	Verification by statistical numerical simulation	50
2.2.3.	Vcm	53
2.2.4.	L and VCR.....	53
2.2.5.	SDDxx and SCCxx.....	53
2.3.	TIME DOMAIN METHODOLOGY USING TDT MEASUREMENT	54
2.3.1.	dWDP	54
2.3.1.1	Measure the step response by TDR instrument	54
2.3.1.2	Shift and add step response.....	55
2.3.1.3	Take the optimized TDR/TDT measurement	55
2.3.2.	NEXT	56
2.3.2.1	Measure the step response by TDR instrument	56
2.3.2.2	Apply statistical estimation using pulse response.....	56
2.3.3.	Vcm	57
2.3.4.	L and VCR.....	57
2.3.5.	SDDxx and SCCxx.....	57
2.4.	VALIDATION OF NOVEL TIME DOMAIN METHODOLOGY.....	58
2.4.1.	dWDP	58
2.4.2.	NEXT	59
2.4.3.	Vcm	60
2.5.	CONCLUSION.....	61
2.6.	CABLE CERTIFICATION TOOL.....	61
	BIBLIOGRAPHY.....	67
	VITA	73

LIST OF ILLUSTRATIONS

Figure	Page
1.1. Definition of the port used for the Z11 calculation.	3
1.2. Structure of the SPICE model with the non-linear arc.	5
1.3. Comparison of $\text{Mag}(Z_{11})$ obtained from different methods.	7
1.4. Comparison of $\text{Real}(Z_{11})$ and $\text{Imag}(Z_{11})$ obtained from different methods.	7
1.5. Equivalent circuit of an ESD generator.	8
1.6. Simulated discharge currents of an ESD generator discharging to a ground plane in air discharge mode at a 5 kV charge voltage.	9
1.7. Comparison of discharge currents discharging to ground plane.	10
1.8. Full wave model of the ESD generator and MP3 player.	12
1.9. Location of the Z11 port.	13
1.10. Simulated Z11 of the ESD generator discharging to a small product.	13
1.11. Simulated discharge current of the ESD generator discharging into the MP3 in the air discharge mode at a 5 kV charge voltage.	14
1.12. Comparison of the port voltage in the SPICE and the CST model of Case I.	16
1.13. Measurement setup.	17
1.14. Measurement setup.	17
1.15. Measured discharge current of short ground strap.	18
1.16. Simulated discharge current for a 0.3 mm arc length and measured current for a fast approach speed.	19
1.17. The comparison of simulated discharge current for a 0.7 mm arc length and measured current for a medium approach speed.	20
1.18. Simulated discharge current for a 1.1 mm arc length and measured current for a slow approach speed.	21
1.19. Measured and simulated magnetic field at 5 cm away from the discharge point	22
2.1. Building a signal using pulse response.	27
2.2. Building a signal using step response.	28
2.3. Flowchart of getting causal impulse response from band-limited S-parameters.	30
2.4. Comparison of raw data and linear extrapolated data.	31
2.5. Comparison of raw data and vector fitting data.	31
2.6. Impulse response obtained after forcing delay causality and without forcing delay causality.	33

2.7. Find zero-crossing points and extrapolate the real(sdd21) to Nyquist frequency starting from the last zero-crossing point location.	34
2.8. Extrapolate the real(Sdd21) to Nyquist frequency using a constant value.	35
2.9. Comparison between cosine extrapolated and constant extrapolated impulse response.	36
2.10. The original S-parameters.	37
2.11. Comparison between the delay-forced SDD21 and the final causal SDD21.	38
2.12. The causal impulse response waveform.	38
2.13. Comparison of step response and impulse response.	39
2.14. Comparison between frequency domain approach and time domain approach.	40
2.15. Distributions of random variables denoting different groups of samples.....	42
2.16. Illustration of pulse response shifting and superimposition.	47
2.17. Original SDD21 of NEXT S-parameters.	48
2.18. 1e-3 constant extrapolation on SDD21 of NEXT S-parameters.....	49
2.19. Pulse response after constant extrapolation of 1e-3 on SDD21 of NEXT.	50
2.20. Illustration of statistical numerical simulation.	51
2.21. Illustration of how to get all possible combinations.....	52
2.22. Measured TDD21 and cable delay.	54
2.23. Comparison between TD approach using SDD21 and measured TDD21.....	56
2.24. Measured TDD21 step response of NEXT.	57
2.25. NEXT source voltage amplitude (p-p) is 700 mV.	59
2.26. Measured NEXT RMS value is 0.9218 mV.	60
2.27. Cable certification tool main window.....	62
2.28. Options window for setting input data type and specify WDPi.	63
2.29. Signal pattern settings window for setting waveform parameters.....	63
2.30. Add a new cable by importing S-parameters.	64
2.31. Add a new cable by importing CSV files.	64
2.32. A wizard for importing CSV data files.	65
2.33. A wizard for importing TXT data files.	65
2.34. A MATLAB figure based report.	66

LIST OF TABLES

Table	Page
1.1. Four step process for simulating air discharge ESD.	3
1.2. Comparison of arc length effect.	15
2.1. Comparison of dWDP from different methods.	40
2.2. Comparison of FD & TD time consumption.	41
2.3. Comparison of NEXT value from multiple numerical simulations.	52
2.4. Comparison of dWDP measurement results from different pre-emphasis.	58
2.5. Comparison of NEXT evaluation from three methods.	60

1. FULL WAVE SIMULATION OF AN ELECTROSTATIC DISCHARGE GENERATOR DISCHARGING IN AIR DISCHARGE MODE

1.1. INTRODUCTION

Simulating Electrostatic Discharge (ESD) allows predicting the currents and fields seen within a DUT during an ESD, thus it helps to predict failure levels [1], [2]. The most commonly used test standard IEC 61000-4-2 [3] requires using contact mode discharges to metallic surfaces and air discharge mode to non-conducting surfaces. If an air discharge is attempted to a non-conducting surface a discharge to a conducting part can occur.

In contact mode the output wave form is proportional to the charge voltage, thus, the ESD generator can be analyzed as a linear system in both time and frequency domain [4]. Those models differ in the software used, the upper frequency limits, and if a specific commercial model of an ESD generator is simulated. However, the numerical modeling of an air discharge is more complex due to the highly non-linear behavior of the arc [9]-[14]. The generator needs to be separated into the linear sections comprising the metallic elements, resistors, capacitors, and the non-linear arc. It has been shown that the arc can be modeled as a time varying resistor valid for the first 10's of nanoseconds [13]. This model needs to be integrated into the numerical model.

Air discharge currents repeat badly. Even if the voltage and speed of approach are kept the same, ESD currents will vary strongly from discharge to discharge. The variations are due to different arc lengths and not a direct result of corona or speed of approach [13]. Reference [12] shows a method to combine the arc model from Rompe and Weizel with an equivalent circuit of the discharging object. This methodology is expanded in this paper to combine a linear full wave model of the ESD generator and the Device Under Test (DUT) with a non-linear arc model. Currents and fields are obtained.

Section 1.2 introduces the methodology. Sections 1.3 and 1.4 verify the methodology by comparison to measured data. Section 1.5 discusses the application and the limitations of this method.

1.2. METHODOLOGY

In general, different processes are possible for coupling SPICE to a full wave solver: Simultaneous solution exchange voltage and current information with a SPICE like solver after every time step of the full wave solution [15], [16]. Sequential solutions first calculate the S-parameters of the linear section of the circuit and then combine them with the nonlinear part of the circuit in SPICE. We use the second method. It allows re-using the S-parameters to save calculation time if only the arc parameters are changed.

More in detail, a four step process is used which simulates linear parts in full wave and non-linear in SPICE. The arc attaches at two points: At the ESD generator tip and at the DUT. These two points are used to define a port. In the first step the impedance at this port is calculated. This is the impedance looking into the DUT and a Noiseken ESD generator (ESS-2000). The simulation is performed using CST [17]. Both the TD (time domain) and FD (frequency domain) solver can be used. Although the impedance Z_{11} is calculated in the full wave model for a given distance (0.7 mm) between the ESD generator and the DUT, different distances will influence the result little as long as the distance is in the arc length range (0.3 mm to 3.0 mm). The tip to ground capacitance is small relative to the distributed capacitance of the rod. This impedance is transformed into a form suitable for time domain simulation. Here the commercial software Broadband SPICE [21] was used. An order of 28 was selected to generate the circuit. SPICE then combines the impedance description from step 1 with an arc model based on the law of Rompe and Weizel. This law describes the arc during the first 10's of nanoseconds as a resistance and has been validated for ESD applications [18], [19]. The resulting current is re-imported into CST as the excitation waveform of the current port which is placed between the two points that had been previously selected to define the impedance port to calculate Z_{11} (as shown in Figure 1.1) to obtain fields and currents within the ESD generator and the DUT. The process is summarized in Table 1.1.

The detailed combination in SPICE is now shown. The Z_{11} describes the linear part of the system. Once the Z_{11} has been obtained, it needs to be transformed into a form suitable for time domain simulation. Software tools like IDEM [20] or Broadband SPICE [21] have been used successfully in this research. The sub-circuit created from

Z_{11} is not unique. Its complexity can be user defined which depends on the transformation algorithm, the error, and the order of interest.

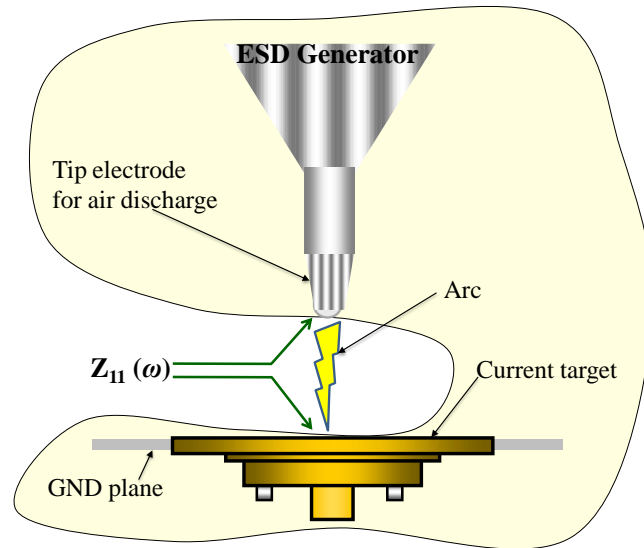


Figure 1.1. Definition of the port used for the Z_{11} calculation.

Table 1.1. Four step process for simulating air discharge ESD.

Step #	Method Description
1	Obtain Z_{11} from the two points at which the arc attaches (looking into ESD generator and the DUT) using a full wave model. The DUT's inner details are not of concern in this step, as one only needs to know the impedance seen by the spark.
2	Obtain a time domain simulation suitable description of Z_{11} . The IDEM (Identification of Electrical Macromodels) tool [20] and Broadband SPICE [21] have been utilized.
3	Combine the equivalent sub-circuit with the arc length model in SPICE to simulate the time domain discharge current waveform.
4	Re-import the discharge current waveform $[I(t)]$ back into the full wave model as a port excitation signal and simulate $V(t)$ (for verification against the $V(t)$ obtained from SPICE), $E\text{-field}(t)$, and $H\text{-field}(t)$ in the full wave simulation. In this step a much more detailed model of the DUT can be used.

The arc of an ESD can be modeled by breaking it down into different phases. The first phase is the resistive phase. The arc is best modeled by a time varying resistance. In the second phase, which is usually reached after a few 10's of nanoseconds, the impedance of the external circuit is larger than the impedance of the arc. In this case the arc often acts more as a constant voltage drop of about 25 V-40 V. The rising edge of the ESD is the main contributor to radiated and inductive coupling into DUTs. For that reason, we concentrate on the resistive phase and do not model other aspects (e.g., how the arc extinguishes). Multiple models describe the resistive phase or arcs [18], [19], [22]. In [13], it has been shown that the model of Rompe and Weizel's is most suitable for ESD simulation as it can correctly describe the effect of the arc length on the rise time and peak current. The arc resistance can be calculated by (1) [13]:

$$R(t) = d / \text{sqr}(2a \int_0^t i(\xi)^2 d\xi) \quad (1)$$

where R is the arc resistance (Ω), d is the arc length (m), a is the empirical constant, most empirically derived values are $a = (0.5-1) \times 10^{-4} \text{ m}^2/\text{V}^2\text{s}$ and i is the discharge current (A).

The structure of the SPICE model is shown in Figure 1.2. A step function having a rise time of approximately 30 ps was used as the source. The rise time is selected by two criteria: If it is too long, then it will influence the current rise time. The current rise time should be determined only the arc resistance law and the linear equivalent circuit. Further, the rise time cannot be too small, if the pulse contains strong frequency components beyond the range in which the impedance is calculated it can lead to instabilities in the SPICE simulation. The fast voltage rise starts the arc resistance model. The current rise time is not determined by the rise time of the step function, but by the arc resistance model. The subcircuit represents Z11. The user provides the voltage and the arc length to calculate the discharge currents. The longest possible arc length in a homogeneous field is given by the Paschen law [13]. Such arc lengths would occur in air discharge for low approach speeds or in humid air conditions. The long arc length leads to slow rise times and lower peak values. Longer arc lengths than the length given by Paschen's equation are possible in strongly non-homogeneous fields, e.g., if the discharge is between an ESD generator and a sharp edged metal part or if the discharge is gliding on a non-conducting surface. Very short arc lengths occur at high approach speeds and in dry air [9], [13], [23], leading to fast rise times and very high peak current values.

In the following this methodology will be first applied to a discharge to a ground plane, mainly for verification purposes, and then to a discharge to a small MP3 player.

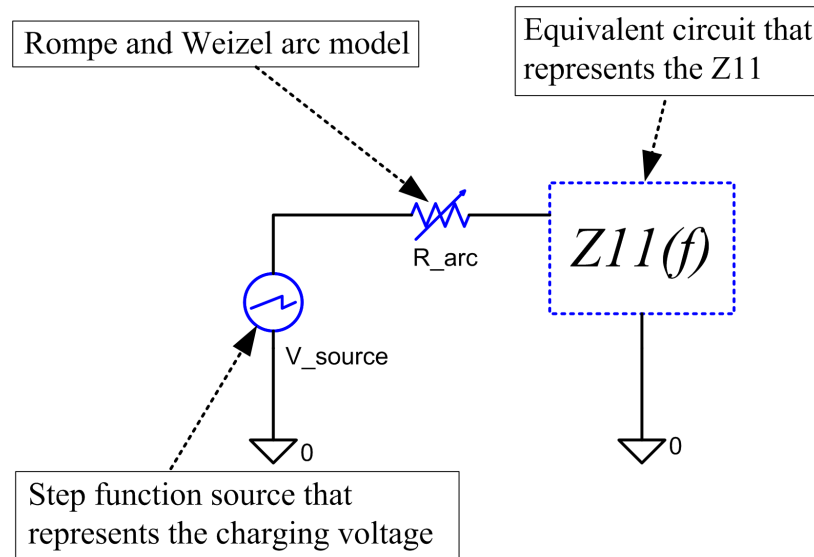


Figure 1.2. Structure of the SPICE model with the non-linear arc [12].

1.3. CASE 1: ESD GENERATOR DISCHARGE TO A GROUND PLANE

1.3.1. Z11 Between the Tip of the ESD Generator and the Ground Plane. The structural and discrete elements of the ESD generator are linear with respect to voltage. We further assume that the DUT acts linearly. For obtaining the current injected by the arc, this does not require that no non-linear effects take place inside the DUT; it only requires that the current injected into the DUT is proportional to the charge voltage. For example, if an internal ESD protection device would clamp a trace voltage while the ESD current is injected into the ground system of the DUT, then this clamping would have hardly any effect on the current, thus, the DUT would act as a linear device as seen by the ESD generator. However, if secondary breakdown occurs, e.g., a spark within an attached 2-wire power supply, then this could strongly affect the ESD current, thus the modeling approach might lead to wrong results.

Both time and frequency domain solvers can be used to obtain Z11. We observed the frequency domain simulation giving a more reasonable Z11 result and using less simulation time. The simulated Z11 for the structure of the ESD generator above a ground plane is shown in Figure 1.3 and Figure 1.4 as the dotted line. This result is verified by comparison with measurement and an approximate SPICE model of this ESD generator [4]. The model contains sufficient detail for achieving a good match to measured impedance data, and correctly represents the 110 pF capacitor and 330 Ω resistor structure inside the ESD generator at lower frequencies. The calculation takes about 15 hours on a PC (CPU 3.20 GHz, 16G RAM).

ESD generators have long ground straps. It increases the simulation time if the full length is included into the simulation domain. As most disturbances are caused by the fast changing parts of the currents and fields, one may not need to include the full ground strap into the model. The ground strap mainly influences the falling part of the waveform. The SPICE model shown in Figure 1.5 includes a 3500 nH inductor to model the ground strap. A shorter ground strap will reduce the time between the first and the second peak of the discharge waveform.

The first step obtained the impedance representing an ESD generator discharges to a large ground plane. In the next step the impedance is transformed into the time domain suitable form and combined with a nonlinear arc equation in SPICE.

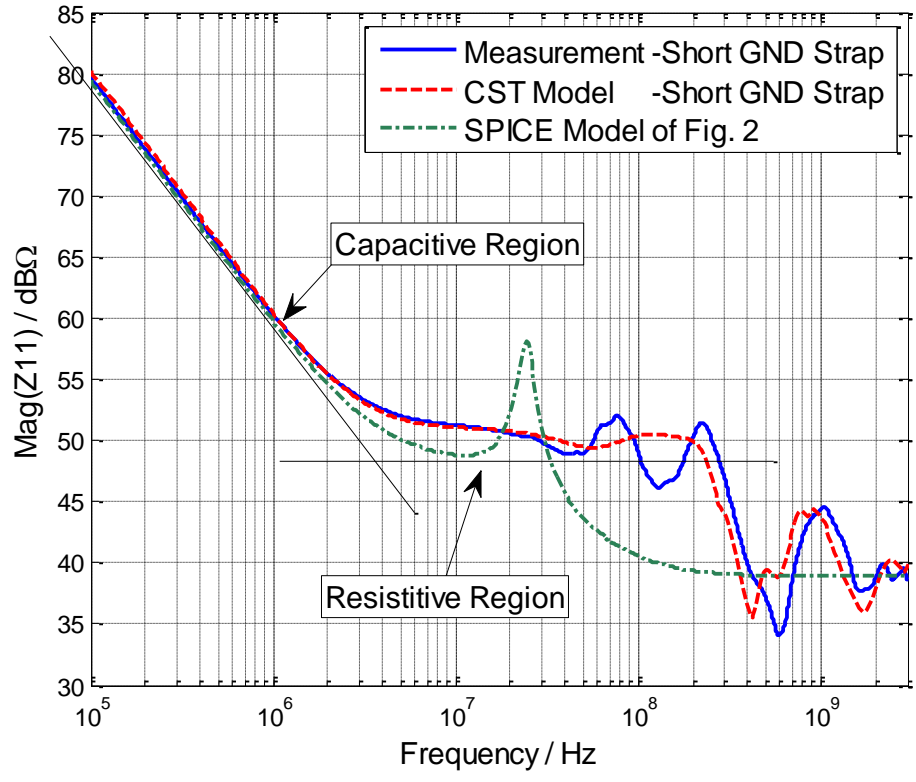


Figure 1.3. Comparison of $\text{Mag}(Z_{11})$ obtained from different methods.

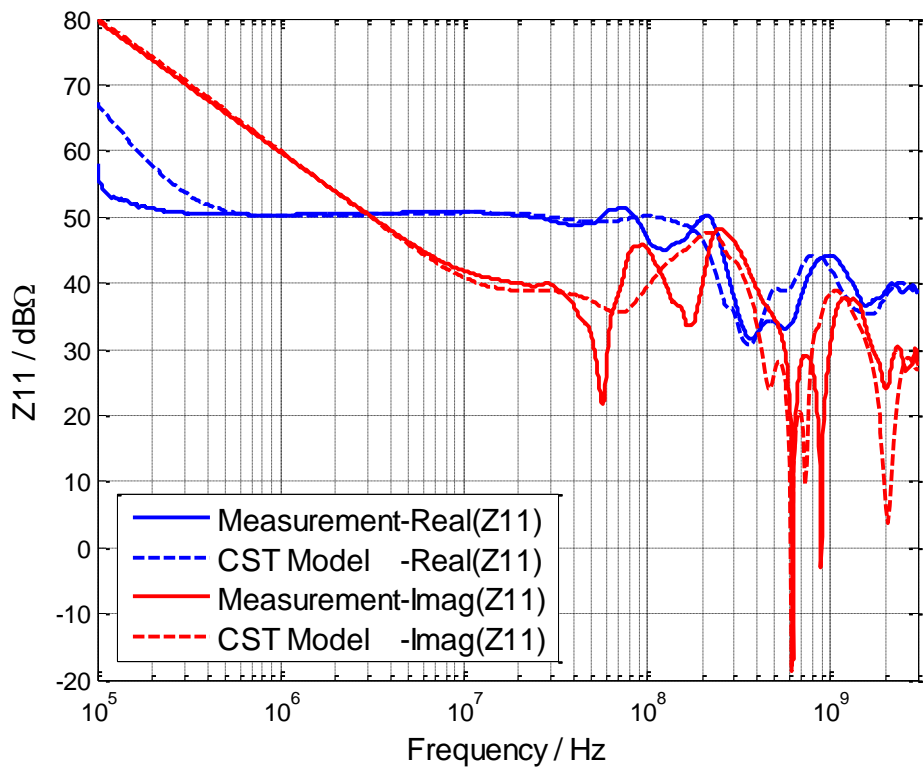


Figure 1.4. Comparison of $\text{Real}(Z_{11})$ and $\text{Imag}(Z_{11})$ obtained from different methods.

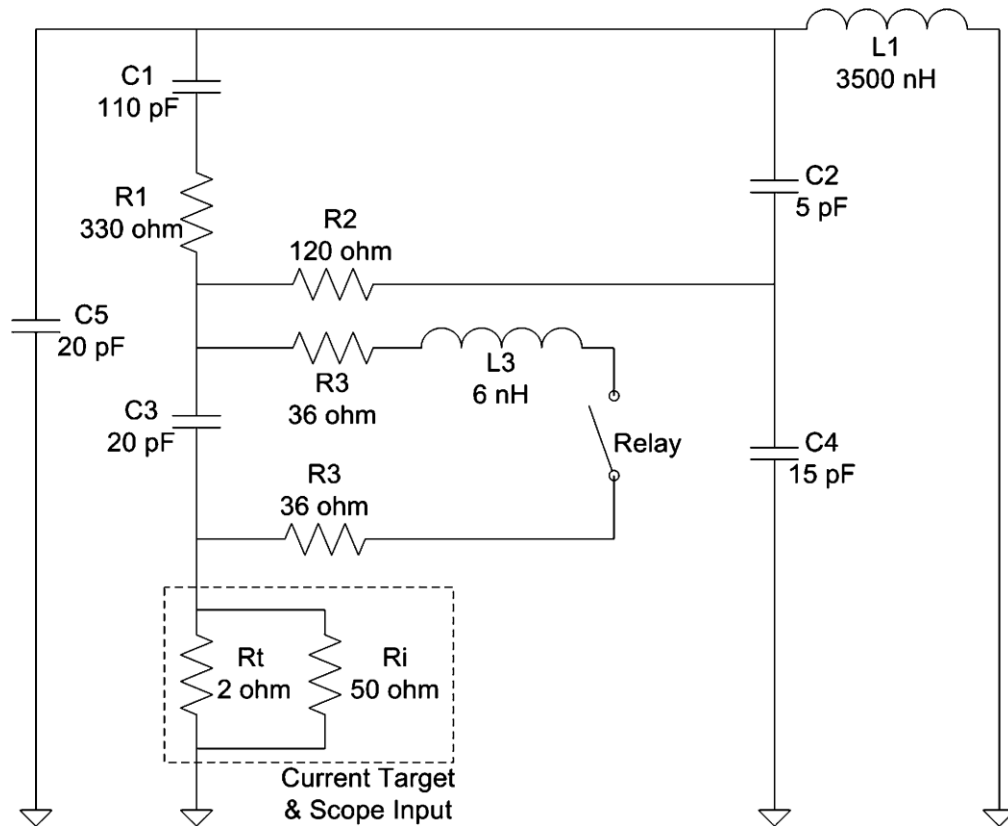


Figure 1.5. Equivalent circuit of an ESD generator [4].

1.3.2. SPICE Simulation for the Discharge Current. Figure 1.6 illustrates the effect of the arc length on the current waveform. It shows SPICE simulated discharge currents for a 5 kV charge voltage. An arc length of 1.1 mm equals the Paschen length, such a discharge current would be expected at high humidity and slow approach speeds. A more typical value at moderate approach speeds is 0.7 mm. At this value the rise time will be somewhat similar to the rise time of an ESD as given in the IEC 61000-4-2 standard (about 850 ps). A more extreme case is given by the 0.3 mm arc length simulation. Very dry air and high approach speeds might lead to such a discharge. The simulated current peak value is 26 A and the rise time is 150 ps.

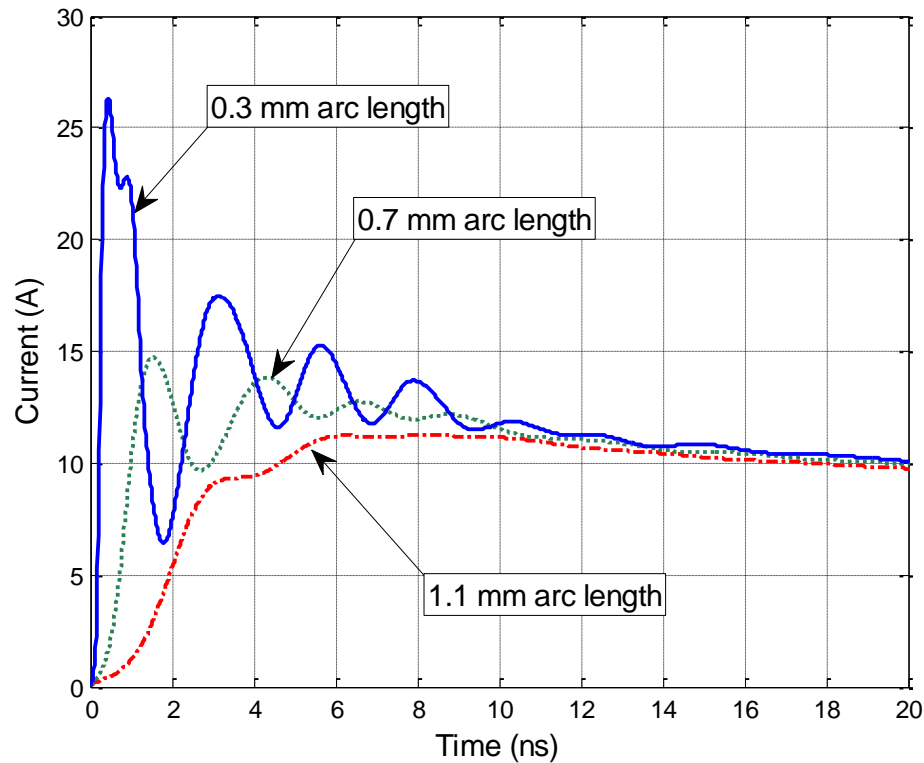


Figure 1.6. Simulated discharge currents of an ESD generator discharging to a ground plane in air discharge mode at a 5 kV charge voltage.

1.3.3. Re-import of Currents into CST. For obtaining the fields, one needs to re-import the discharge current into the full wave model as the excitation waveform. This is discussed and validated in the second case example.

1.3.4. Validation by Measurement Results. The current into the large ground plane was measured using an ESD current sensor as described in [3]. In Figure 1.7, the SPICE simulated discharge currents are compared to the measured data for different approach speeds. Even if the exact approach speed or arc length are not known, it shows that the ranges of arc lengths used in the simulation are representative for discharge currents obtained in the experiment. A more in-depth comparison based on measured arc length values can be found in [13].

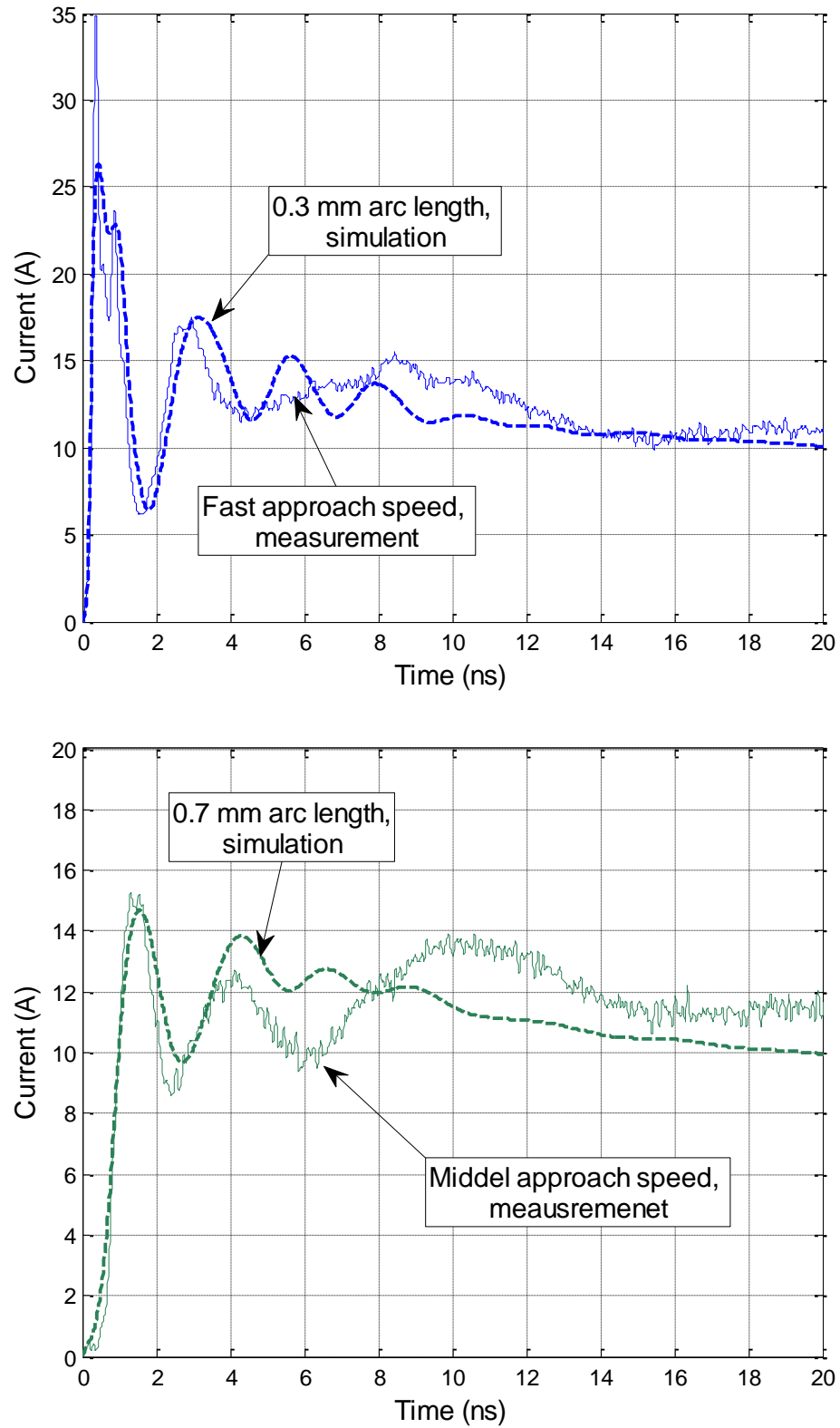


Figure 1.7. Comparison of discharge currents discharging to ground plane.

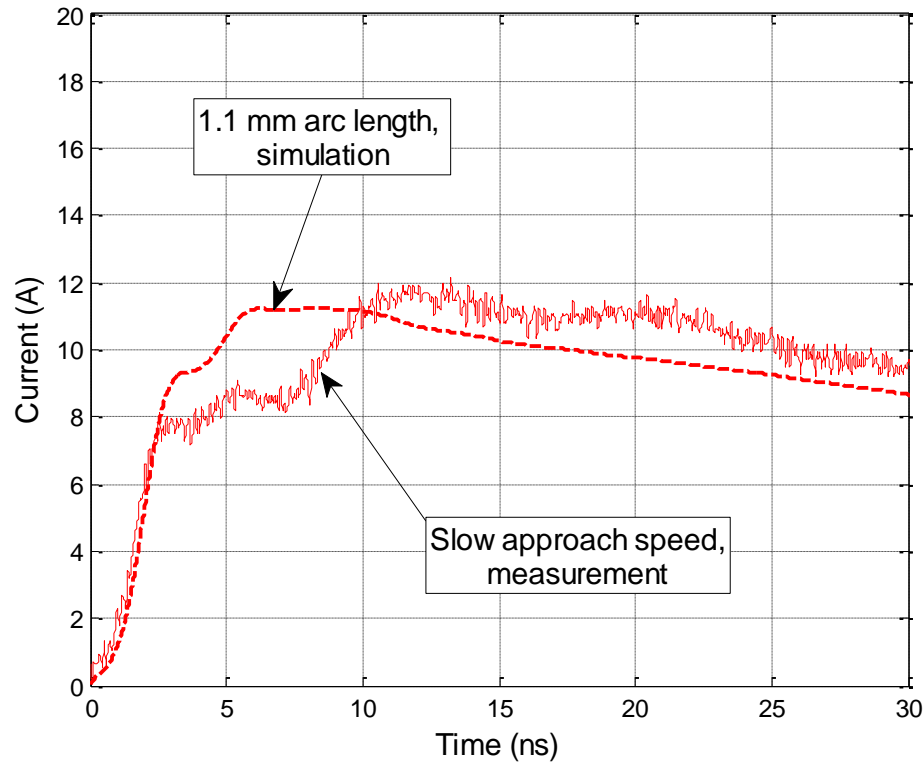


Figure 1.7. Comparison of discharge currents discharging to ground plane (cont.).

1.4. CASE 2: ESD GENERATOR DISCHARGE INTO A SMALL PRODUCT

1.4.1. Z11 Between the Tip of the ESD Generator and the Product. This case simulates a discharge into an MP3 player, a small, non-grounded DUT. The whole geometry is shown in Figure 1.8. The MP3 player model includes the main blocks of the DUT similar to [24]. In brief, the major blocks of the player (metal frame, battery, display, PCBs) are modeled as metal blocks connected at locations of connectors and frame connection points.

The DUT is placed on a dielectric sheet above a larger ground plane. This forms a capacitor having a capacitance of about 25 pF, leading to a higher value of Z11 at lower frequencies. The value for Z11 was obtained as shown in Figure 1.9. The comparison between Z11 of the ESD generator and the large ground plane and Z11 of the ESD generator with the MP3 player is shown in Figure 1.10. It mainly shows the smaller capacitance at lower frequencies; at higher frequencies the impedance of the 25 pF

capacitor formed by the player against the ground plane is lower than the source impedance of the ESD generator, thus the impedance in case 2 is similar to the impedance seen in case 1, the discharge to a large ground plane.

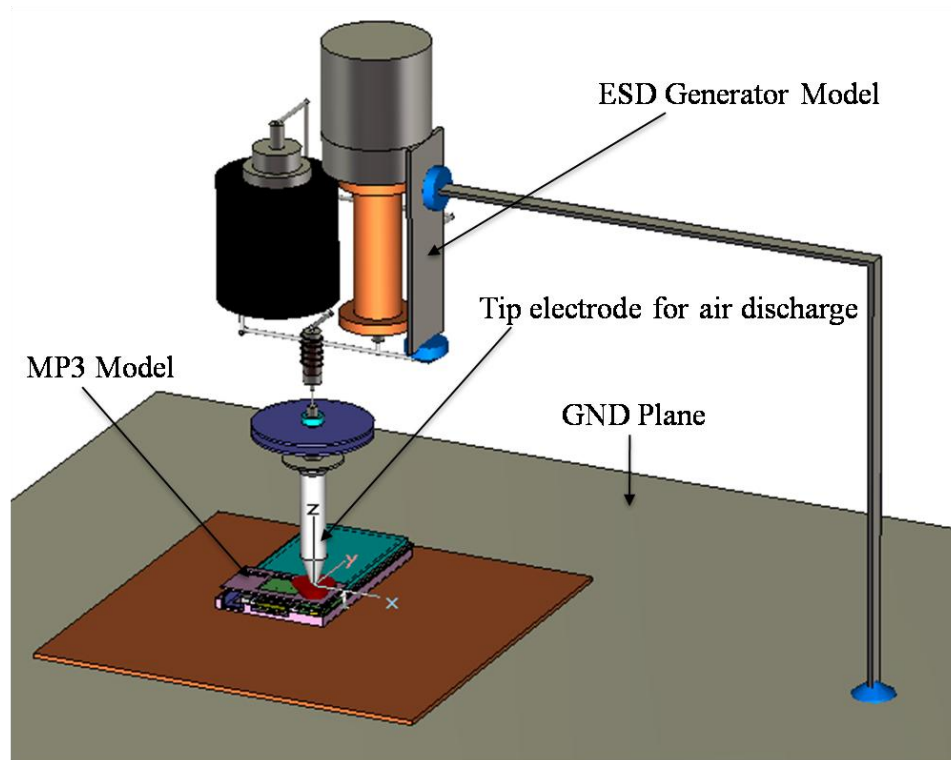


Figure 1.8. Full wave model of the ESD generator and MP3 player.

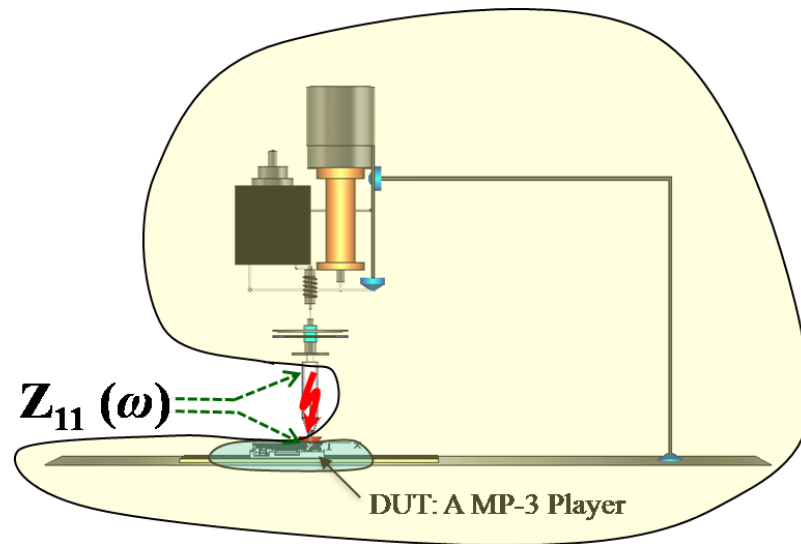


Figure 1.9. Location of the Z11 port.

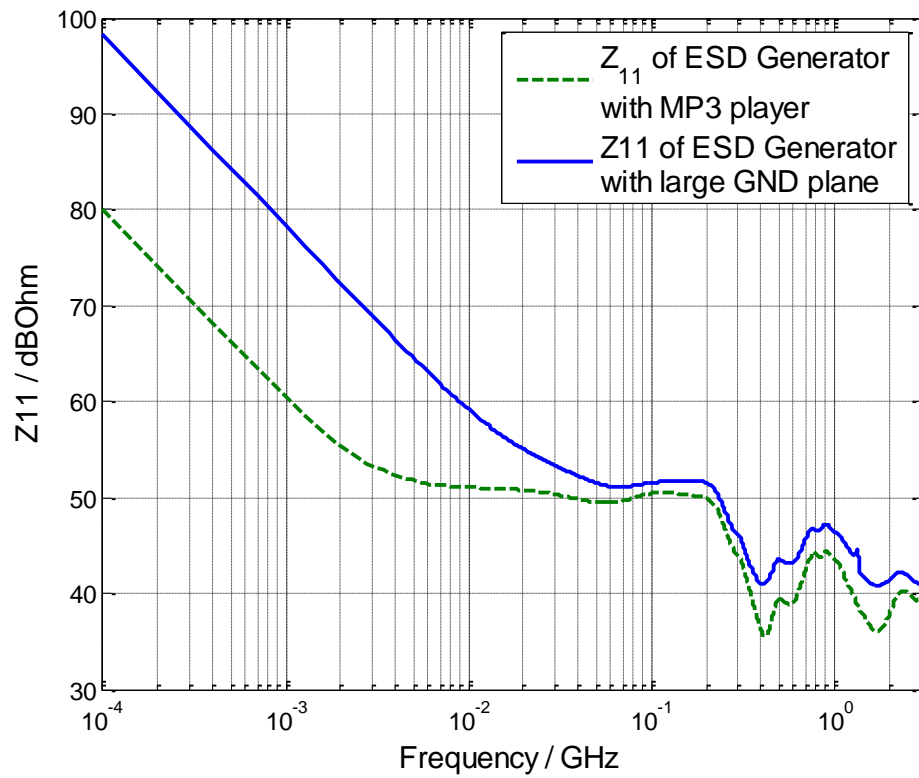


Figure 1.10. Simulated Z_{11} of the ESD generator discharging to a small product.

1.4.2. SPICE Simulation for the Discharge Current. The Z11 defined between the discharge tip and the MP3 player was transformed into a subcircuit using Broadband SPICE. The subcircuit combined with the arc model gave the simulated discharge current for different user-defined charging voltage and arc length. The simulated discharge current at the 5 kV charge voltage with different arc lengths is shown in Figure 1.11.

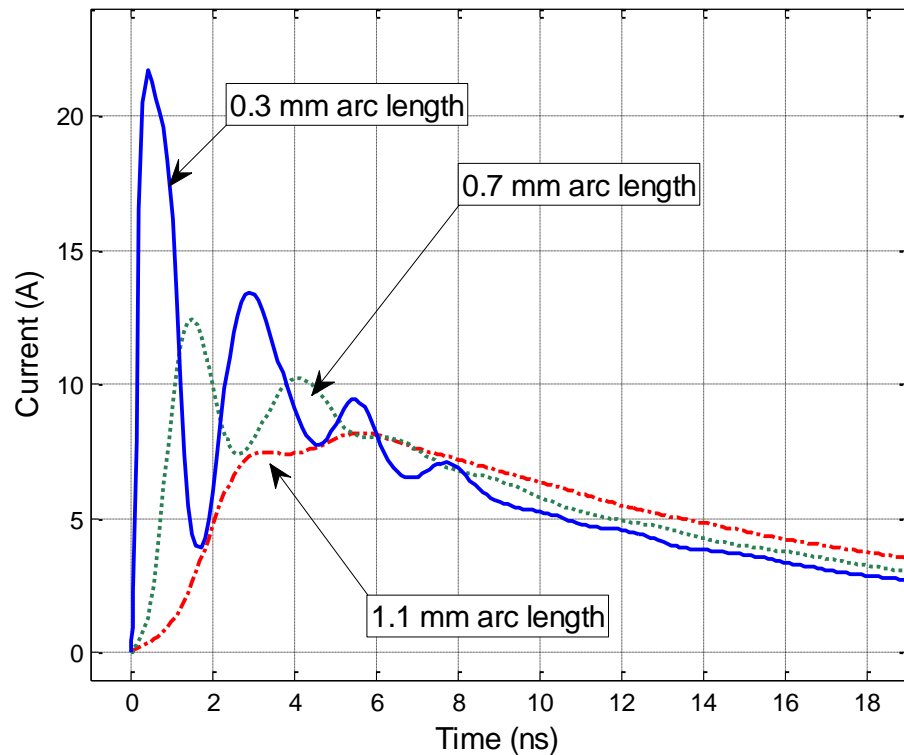


Figure 1.11. Simulated discharge current of the ESD generator discharging into the MP3 in the air discharge mode at a 5 kV charge voltage.

The obtained peak values and rise times are tabulated in Table 1.2. The arc length has a very strong effect on the parameters shown, especially, the current derivative.

Table 1.2. Comparison of arc length effect.

Arc Length	peak value (A)	rise time (ps)	max di/dt (A/ns)
0.3 mm	21.7	200	105.19
0.7 mm	12.4	780	16.617
1.1 mm	8.1	2260	4.5170

1.4.3. Re-import of Currents into CST. To obtain transient fields the current waveform obtained from the SPICE simulation is re-imported into CST as the excitation waveform. The current source port is placed between the two points that had been previously selected to define the impedance port to calculate Z11. One check is worthwhile: If the Z11 representation used in SPICE would perfectly match the Z11 from the frequency domain full wave simulation then the port voltage obtained during the full wave simulation using the re-imported current would match the port voltage (=voltage across the arc) in the SPICE simulation.

For Case II, the SPICE simulated current was imported back to the CST model as the current source. The comparison of the port voltage in the SPICE model and the port voltage in the CST model in Figure 1.12 shows a good match.

The simulation using the re-imported current allows simulating the fields within and around the MP3 player by placing appropriate monitor probes. If these probes are placed close to the metallic surfaces of the MP3 player, then they represent the surface current densities and the displacement current densities which can be used to estimate the coupling into bond wires of an IC, traces, and flex cables for predicting ESD upset threshold levels. Before current and field results are shown, the measurement methods are introduced.

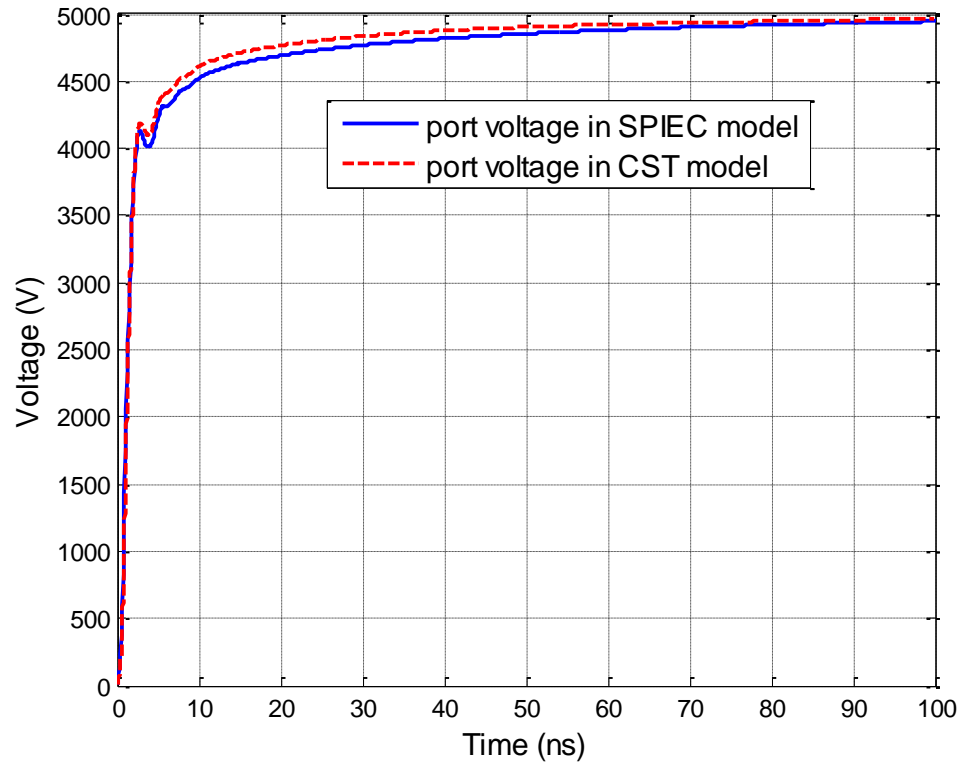


Figure 1.12. Comparison of the port voltage in the SPIEC and the CST model of Case I.

1.4.4. Validation by Measurement Results. The current was injected into the small product and the magnetic field was measured. To capture the current injected into the MP3 player, an F-65 (1 MHz – 1 GHz) current probe was used as shown in Figure 1.13. The magnetic field was measured using a small shielded loop and a Tektronix 7404 (4 GHz BW, 20 GS/s) oscilloscope.

At 5 kV charge voltage, a NoiseKen ESD generator was discharged into the player. The player was placed above a large GND plane with a dielectric sheet between them. Figure 1.13 and Figure 1.14 illustrate the setup.

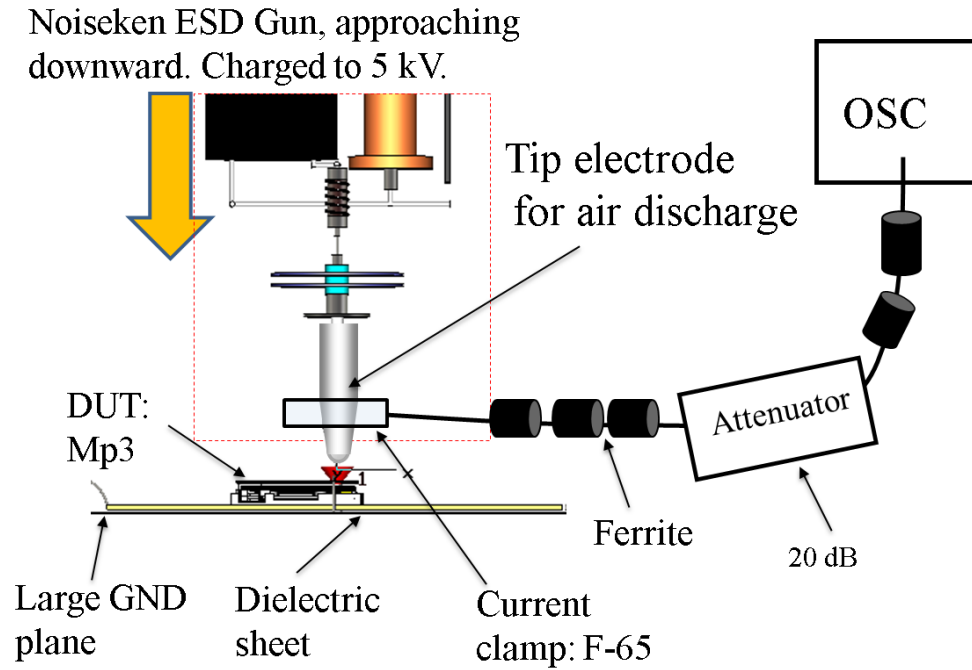


Figure 1.13. Measurement setup. The F-65 current clamp was placed around the discharge tip and above the product.

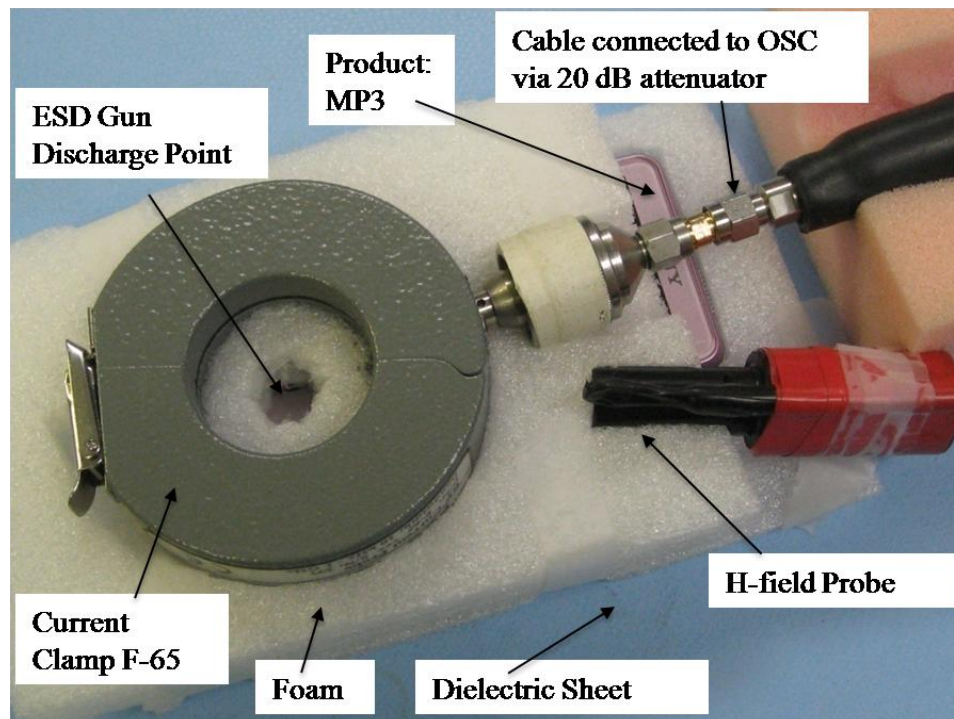


Figure 1.14. Measurement setup.

The relationship between approach speed, humidity, and arc length is not of deterministic nature, but given by the influence of the humidity on the statistical time lag [13]. Thus, on average one will observe shorter arc lengths with increasing approach speeds for a given charge voltage. For achieving short arc length discharges without reducing the humidity, the surface had been cleaned using alcohol and fast approach speeds have been used, longer arc lengths are achieved by slow approach speeds. Shown are examples of the captured waveforms for different approach speeds.

1.4.4.1 Measured discharge current. The current clamp's frequency response falls off above 1 GHz bandwidth, thus the fastest rise time of a step response signal would be approximately 300 ps. Figure 1.15 shows measured discharge currents for different approach speeds.

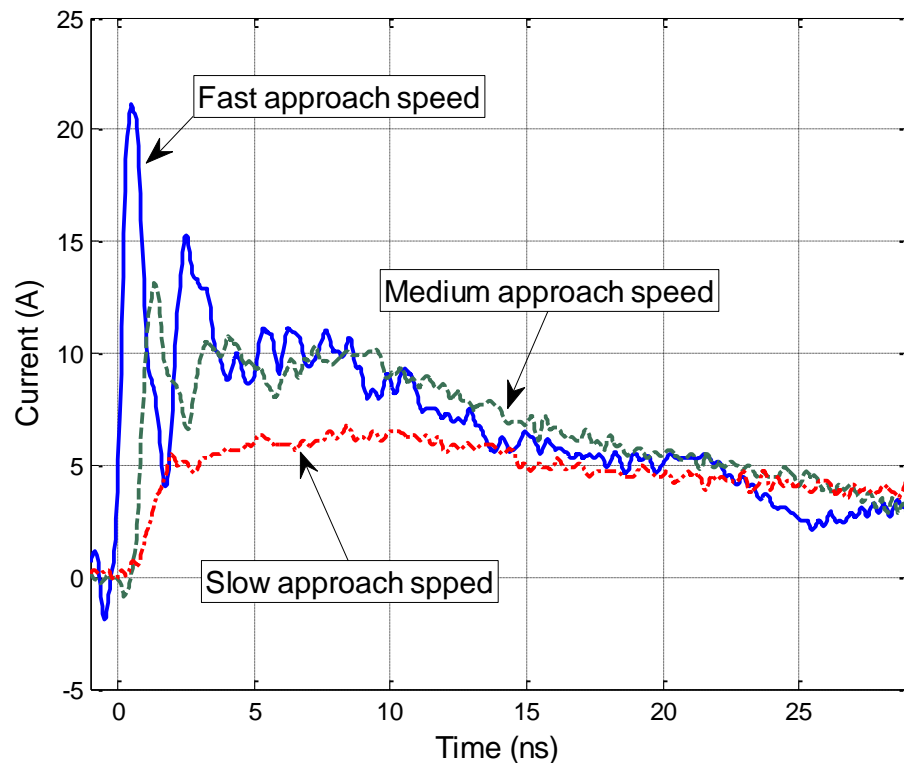


Figure 1.15. Measured discharge current of short ground strap.

The simulation results are compared to the measured results for verification. The fast rise time result is shown in Figure 1.16. The simulated discharge current for a 0.3 mm arc length and 5 kV charging voltage gives a discharge current with a rise time of about 200 ps and a peak value of 21 A. The measured discharge current has a rise time of about 300 ps and a peak magnitude of about 22 A. The difference can be explained by the limited bandwidth of the F-65 clamp. Due to the difficulty in measuring arc length we can only approximately compare measured and simulated results. Nevertheless, the comparison shows that the simulated and measured data are within the same ranges.

In Figure 1.17 and Figure 1.18, the comparison of simulation discharge current for 0.7 mm and 1.1 mm arc length is shown. They match well with the measured results.

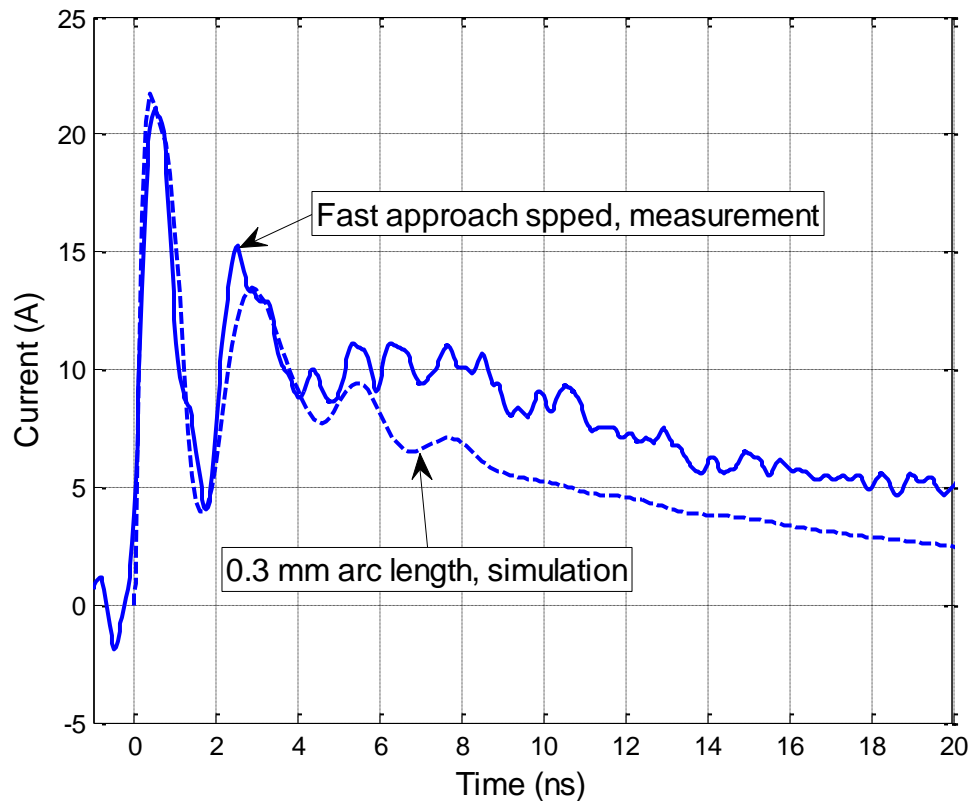


Figure 1.16. Simulated discharge current for a 0.3 mm arc length and measured current for a fast approach speed.

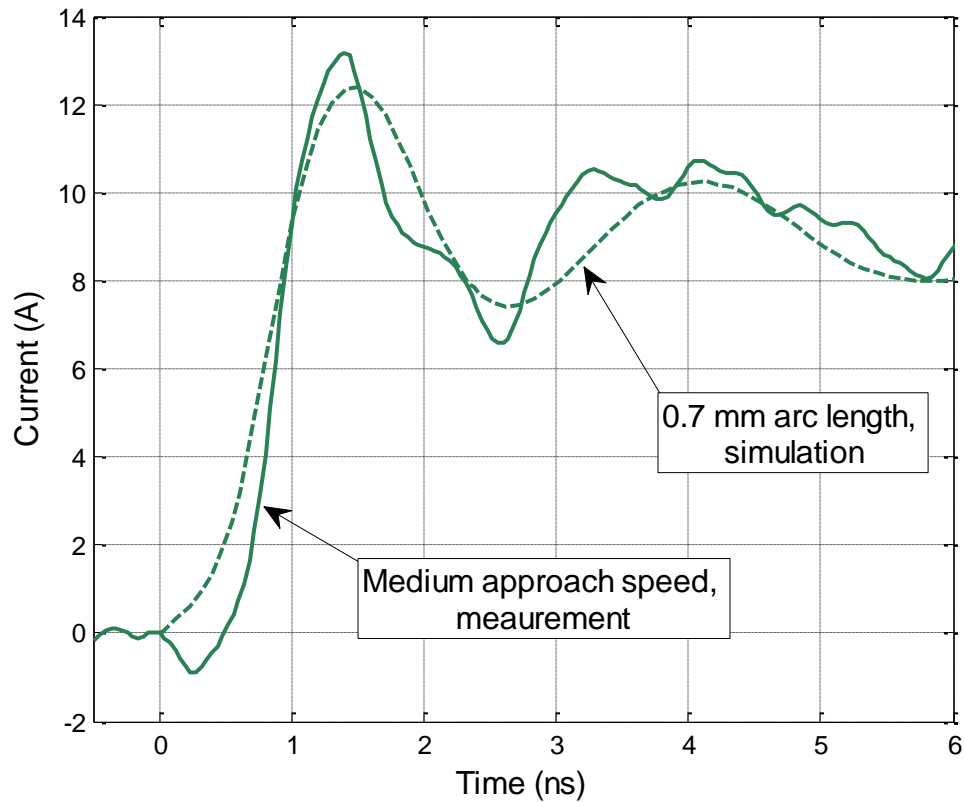


Figure 1.17. The comparison of simulated discharge current for a 0.7 mm arc length and measured current for a medium approach speed.

In measurement, several approaches are measured to choose a best match, since a better way to exactly control the arc length is not developed. In one of the references, a arc length measurement method was developed by Dr. Pommerenke. In Figure 1.18, the measured discharge current 1.1 mm arc length doesn't have the peak as shown in the simulation discharge current, this may be caused by the air environment condition, such as humidity, air pressure, etc.

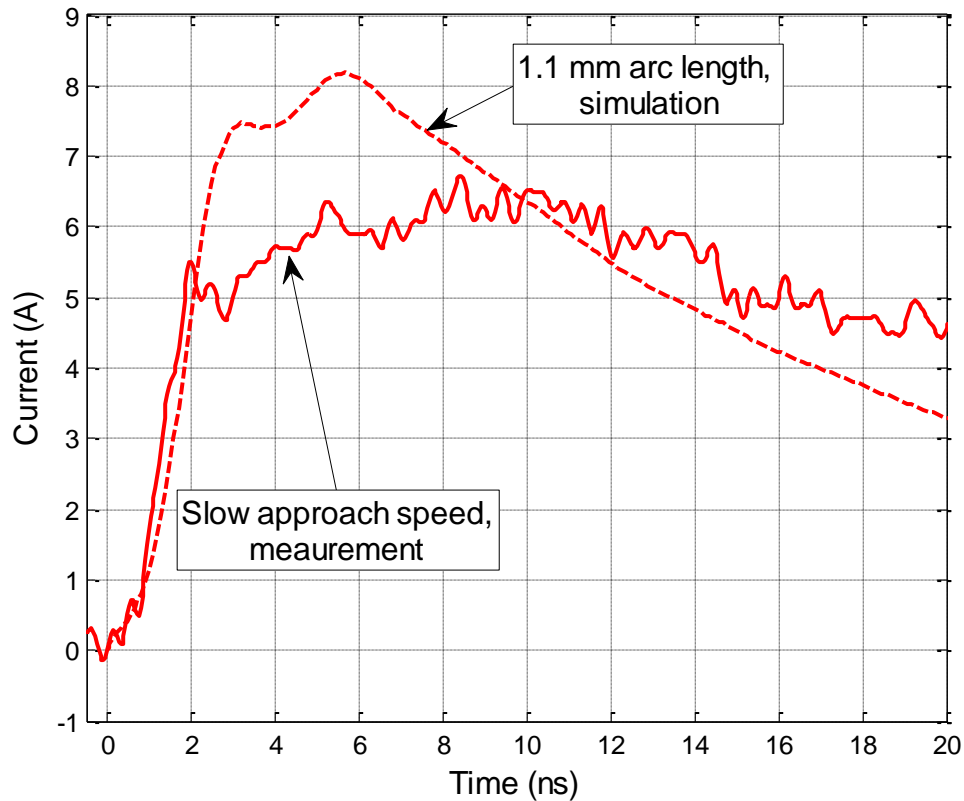


Figure 1.18. Simulated discharge current for a 1.1 mm arc length and measured current for a slow approach speed.

1.4.4.2 Measured magnetic field. This is to confirm the last step of the process: Injecting the SPICE simulated current back into the full wave simulation for obtaining fields. A shielded loop was placed 5 cm away from the product (Figure 1.14). A deconvolution was performed to obtain the field strength from the captured voltage at the probe output. The deconvolution is mainly an integration process, having two deviations from the ideal integration. At lower frequencies high pass filtering is performed to avoid the accumulation of the oscilloscope's small but relevant DC offset during the integration. Second, at higher frequencies the self-inductance of the probe in conjunction with the 50 Ω load, leads to a self-integration thus no external integration is needed above 3 GHz. The resulting magnetic fields are shown in Figure 1.19. The data match well. The measured rise time is about 250 ps. Using the SPICE model one can estimate the arc length from the rise time. Repeated simulations indicate an arc length of about 0.4 mm.

The Paschen length for 5 kV is about 1.1 mm at sea level air pressure. Thus, the combination of the speed of approach and the statistical time lag reduced the arc length in this measurement to 35% of the Paschen value, leading to a very fast rising ESD current.

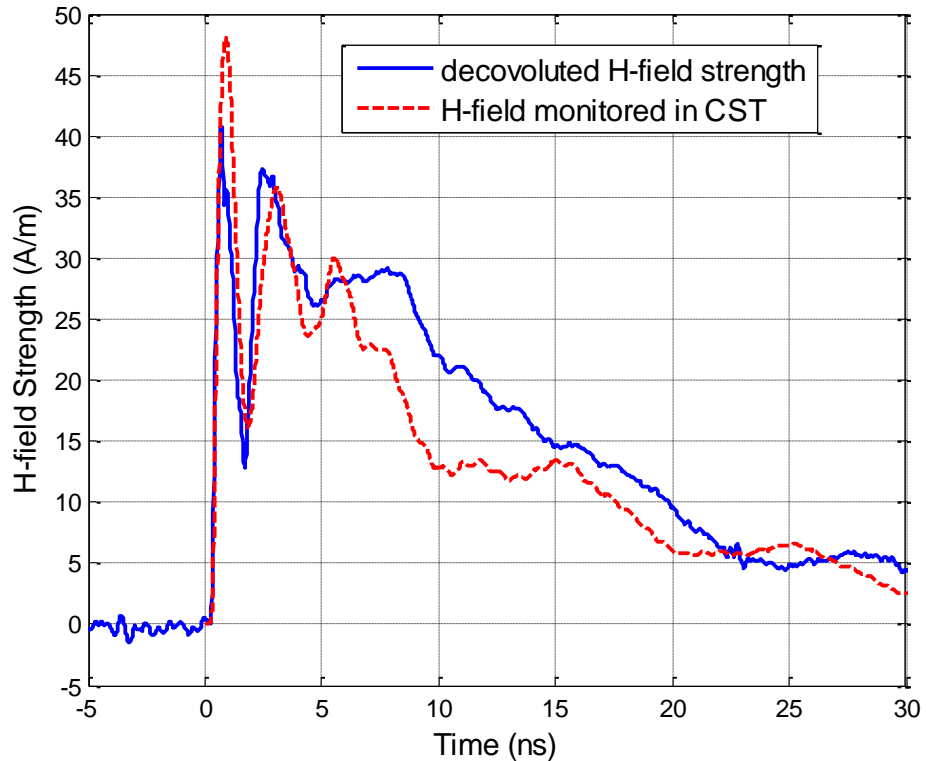


Figure 1.19. Measured and simulated magnetic field at 5 cm away from the discharge point.

1.5. DISCUSSION

The methodology allows predicting the currents and fields in and around a product. There are three types of limitations in the methodology.

The most obvious one results from the limited ability of simulating details in the product and within the ESD generator. As with every simulation, the number of unknowns and the ratio of the smallest to the largest detail will limit the size of the model. The methodology allows circumventing this at least partially, especially for small products. If the product is small, then the fields inside the product will be dominated by

the fields caused from the injected current and not by fields directly coupling from the body of the ESD generator. Those fields would especially be significant in the contact mode in which the field components that are greater than 1 GHz are often caused by the rapid voltage breakdown in the gas filled relay that initiates the discharge. As this analysis is for an air discharge, one will find the strongest high frequency components directly at the arc, as with further distance from the arc high frequency components will be attenuated by both frequency dependent loss and radiation. If the fields are dominated by the injected current, then one can use a relatively simple model of the product just to determine the current, but in the last step, in which the current is re-injected into the product, a more complex model of the product can be used, but a very simple model of the ESD generator (and a forced current).

The second limitation results from the need for providing the arc length for the arc resistance calculation. Although possible, arc length measurements are difficult to implement. In a simulation we suggest the following approach. At first, an arc length should be selected that leads to an air discharge current that is similar to the contact mode discharge current, as specified in the IEC 61000-4-2 standard. For 5 kV this is about 0.8 mm arc length. Values for other voltages can be found in [13]. As a very slow rising current the Paschen value can be selected, leading to discharges of lower severity and as extremely fast rising current a value of about 30 % of the Paschen length is suggested. This value is based on experimental evidence. In measurements that captured the arc length [13] we found it possible even under very dry air and clean surface conditions to obtain arc lengths of less than 30 % of the Paschen value.

The third limitation is related to stability of the time domain SPICE simulation. In this simulation a very rapid change of resistance is combined with a SPICE impedance model created from full wave simulation. If instabilities occur, one should inspect the SPICE model for passivity and causality, in addition one can simulate the discharge using longer arc lengths first, as these show a slower change of the arc resistance.

The main application of this model lies in the simulation of ESD to products. For example, it is known that the arc length tends to be small for fast approach speeds in dry air. The short arc length leads to fast rise times and high peak values. Using this model, one can quantify the fields inside a product for different arc lengths. Further applications

are the simulation of grounding conditions of products on the arc, and thus the current. Further, the model can be extended to the case of secondary breakdown, e.g., an ESD occurs to an ungrounded metal part leading to a second discharge from this ungrounded part to the main part of the DUT.

1.6. CONCLUSION

The article proposes a method for simulating an ESD generator discharging in air discharge mode into a product. The linear and the non-linear part of the problem are separated to simulate the linear part in a full wave solution and the non-linear arc in SPICE. The SPICE results are re-imported into the full wave problem as the excitation. This allows the fields inside a product during an air discharge to be obtained. The method has been verified by comparison of simulated current and transient field results with measurements.

2. CHANNEL PERFORMANCE CERTIFICATION UTILIZING NOVEL TIME DOMAIN CONVOLUTION METHOD

2.1. INTRODUCTION

Passive direct attach copper cables are certificated with a pair of Module Compliance Boards (MCB). The specifications for SFP+ passive cable assemblies, including Voltage Modulation Amplitude (VMA), VMA Loss (L), VMA Loss to Crosstalk Ratio (VCR), Output AC Common Mode Voltage (V_{cm}), and difference Waveform Distortion Penalty (dWDP), etc, may be derived using frequency based methodologies that yield equivalent results e.g., utilizing frequency dependent crosstalk and insertion loss transfer function. However, a novel time domain based method can be applied to get the parameters in a more effective way.

Waveform distortion penalty (WDP), originally used to quantify the performance of an optical transmitter (TWDP), is defined as the difference (in dB) between a reference signal to noise ratio (SNR) and the equivalent SNR at the slicer input of a reference decision feedback equalizer (DFE) receiver for the measured waveform after propagation through a simulated fiber channel [25], [26]. This concept is now developed in the SFP+ passive copper cable specifications to dWDP, the difference between WDP_o and WDP_i [27].

The measurement of dWDP requires a compliance signal generator with adjustable pre-emphasis, rise and fall times, and an oscilloscope that is able to capture the pattern waveform of PRBS9 according to the standard. A frequency domain approach to dWDP eliminates the demand of the high cost compliance signal generator, by measuring the S-parameters of the cable under test using a vector network analyzer (VNA) which is commonly equipped in universities and companies. In the frequency domain approach, the S-parameters, combined with an emulated input signal having a specified data pattern, generates the time-domain output waveform of the channel under test through a link path analysis [28]. The time-domain input waveform is first generated with a specified data pattern (PRBS9 is used in dWDP calculation). Parameters, including bit rate, rise/fall time, high/low voltage levels, number of samples per bit, number of repetitions of the bit pattern, etc., of this input waveform can be defined and adjusted, and then the time-domain input waveform is transformed into the frequency domain through the Fast

Fourier Transform (FFT). Another input needed for the link path analysis is the frequency-domain S-parameters data of the channel under test. The S-parameters need to be extrapolated to DC and interpolated at a preferred frequency sampling rate, to ensure an accurate and meaningful inverse Fourier Transform later on. After the necessary preprocessing, the frequency-domain S-parameter data are multiplied with the frequency-domain input, resulting in the frequency domain output of the channel under test. Inverse Fourier Transform is then employed and the time domain output waveform of the channel under test is obtained [29]. This time domain output waveform is then used to calculate dWDP.

One disadvantage of this frequency domain approach is the increasing memory consumption when the data sequence becomes longer. Since the whole length of sequence must be performed FFT at one time, there are limitations of the sequence length based on different simulation tools. A time domain convolution method can be used to overcome this. From the pulse response theory, as shown in Figure 2.1, the two symbols representing a digital '0' and '1' are time shifted and superimposed to give a resulting signal. All possible ISI combinations are generated and their resulting amplitudes can be observed [30], [31]. The time domain convolution method does not require to manipulate all bits of the input waveform at one time and therefore can generate super long data sequence, also, the time domain method does not need to generate the input waveform, but only need the transition information known as the '0's and '1's, which can further save memory usage. However, this bit-by-bit convolution method will be really time-consuming. A novel convolution method using a step response instead of the pulse response is proposed in this thesis.

Another parameter in SFP+ passive copper cable certification is the Near End Crosstalk (NEXT), which is the RMS voltage measured by a free running (not triggered) oscilloscope in a bandwidth of 12 GHz. The test pattern for NEXT is PRBS31, which is very hard for a frequency domain based link path analysis because of the memory and time usage. PRBS9 can be used for an approximation of NEXT. A novel method based on the statistic theory using pulse response from the crosstalk transfer function is proposed in this thesis.

V_{cm} can be derived in the same way as NEXT, but using SDC21 instead of SDD21. And V_{cm} calculation should count the common mode voltage from both the insertion loss and crosstalk transfer functions.

Section 2.2 illustrates the novel time domain methods using measured S-parameters; Section 2.3 shows the novel method using TDR measured step responses. Section 2.4 validates the novel method by measurement, Section 2.5 gives the conclusion, and Section 2.6 shows a MATLAB based tool with GUI for the cable certification calculation.

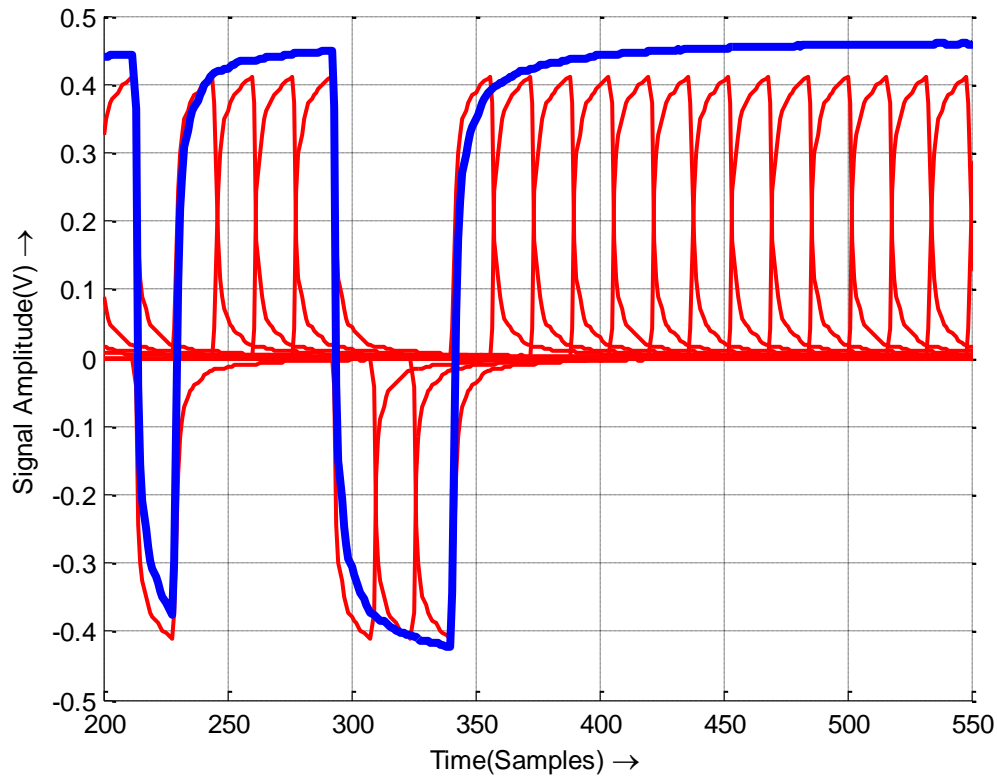


Figure 2.1. Building a signal using pulse response.

2.2. TIME DOMAIN METHODOLOGY USING S-PARAMETERS

All SFP+ passive cable assembly specifications can be derived using time domain method effectively. The proposed method in this section generates step response or impulse response using measured S-parameters, and then applies convolution or statistics.

2.2.1. dWDP. dWDP is calculated by subtracting WDP_i from WDP_o .

2.2.1.1 Using step response. As illustrated in Figure 2.1, an NRZ waveform can be obtained by convolution of the channel PULSE response with data pattern. The bit-by-bit pulse response convolution method requires as many convolving as the data sequence length. The novel method using step response only considers the rising edges and the falling edges. The new method says whenever there is a transition (from '0' to '1' or from '1' to '0'), a step response is convoluted to the transition location, and therefore, the convolving numbers are significantly reduced. Take PRBS9 signal for example, the total transition numbers is 256 while the total bits is 511, so the simulation time can be cut into half. Figure 2.2 shows the same signal built from the step response compared to pulse response in Figure 2.1.

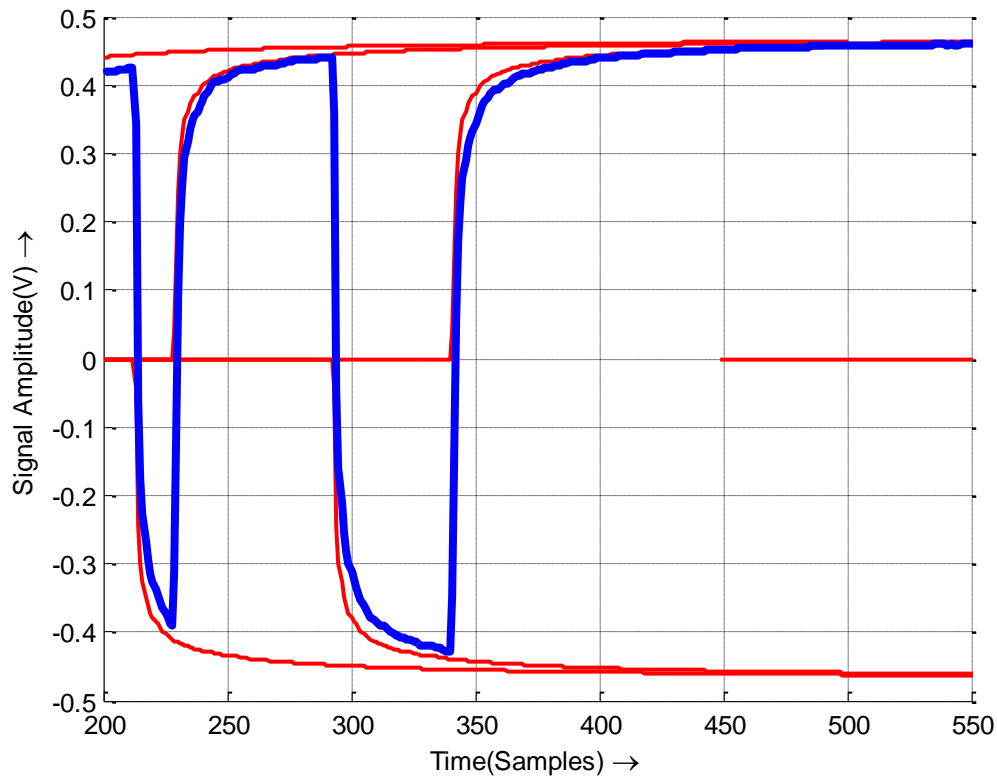


Figure 2.2. Building a signal using step response.

Another more important characteristic of the NRZ sequence is that a ‘0’ to ‘1’ transition is always in pairs with a ‘1’ to ‘0’ transition. As long as the step response goes to steady state, the steady parts of the ‘rising’ step response and the ‘falling’ step response will cancel out and therefore no need to calculate. The simulation time will be further reduced.

2.2.1.2 Get causal step response from S-parameters. There are two methods to get a step response. One is from the measured or simulated S-parameters, while another is directly from the TDR measurement.

Multiple useful references are talking about how to get a casual and passive impulse response from the band limited S-parameters [32]-[49]. Basically, the band limited S-parameters were properly extrapolated to DC and the Nyquist frequency, and then forced delay causality to get the causal impulse response. The impulse response is then convolved with an ideal step waveform with specific rise time (in dWDP calculation, the rise time is set to 34 ps based on SFF-8431 standard) to get the step response. The flowchart of this process is shown in Figure 2.3.

Multiple methods can extrapolate SDD21 response to DC [32]-[37]. A commonly used simple method is the standard linear/spline extrapolation. That the DC value for the phase or imaginary part of the frequency response is zero makes the linear/spline extrapolation easier. A guess of the magnitude or real value at DC also helps. Usually a value of “one” is used for a S21 transfer function.

A better method is to use K-K relationship calculate the real (imaginary) part of the frequency response after the imaginary (real) part was extrapolated [36]. This method enforces the causality on the extrapolated part, but it is based on an assumption that the real (or imaginary, whatever the one used for input of the causality enforcement) is correct, which is not guaranteed by the linear/spline extrapolation. Another method uses an iteration process to refine the extrapolated real and imaginary part based on the K-K relationship, but this method cannot ensure the convergence during the iteration.

A more popular method is the vector fitting algorithm [37]. By finding out the poles and residues of the system, the DC and low frequency response can be extended naturally by the rational polynomial approximation. A comparison between the linear

extrapolation and vector fitting extrapolation method is shown in Figure 2.4 and Figure 2.5.

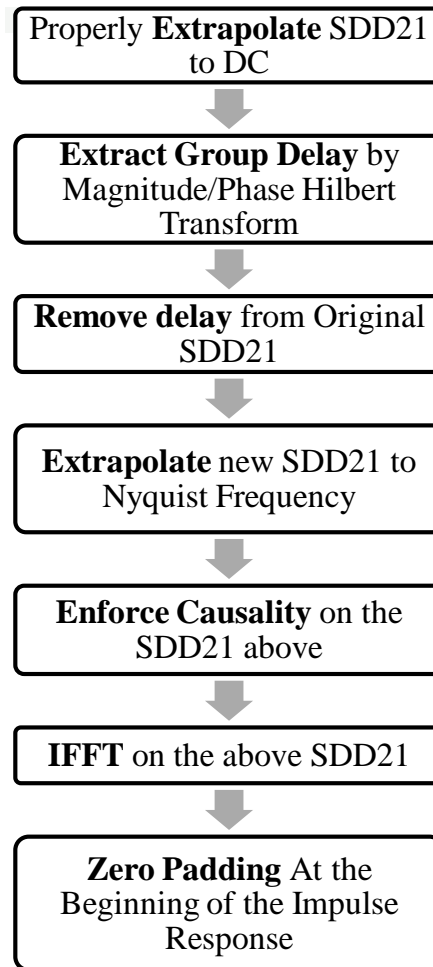


Figure 2.3. Flowchart of getting causal impulse response from band-limited S-parameters.

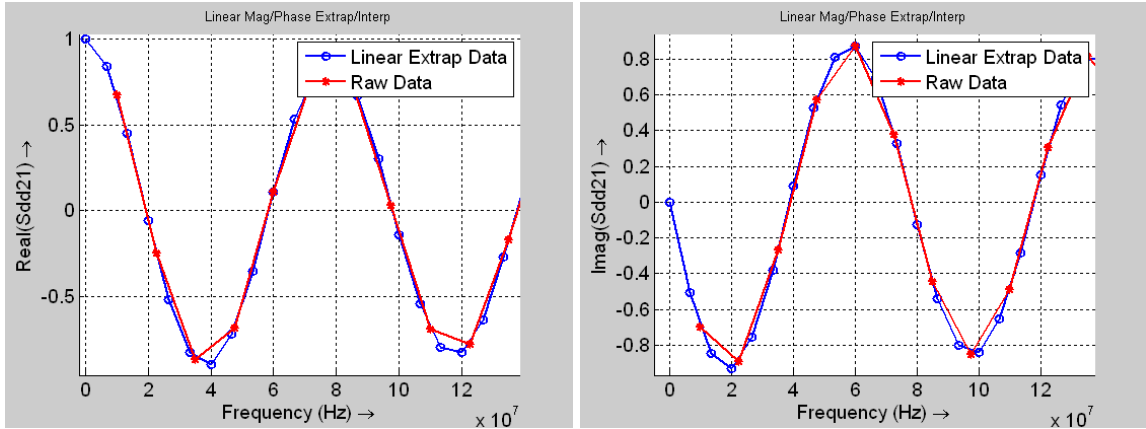


Figure 2.4. Comparison of raw data and linear extrapolated data.

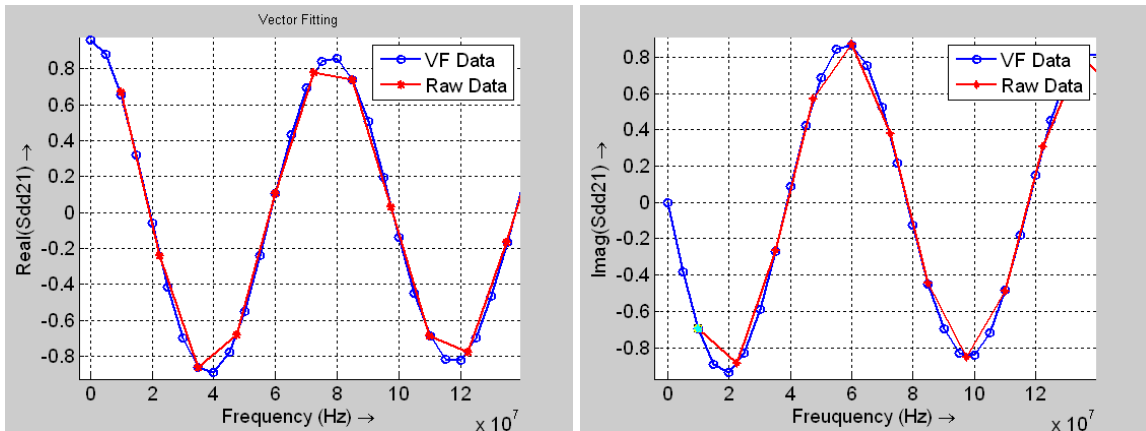


Figure 2.5. Comparison of raw data and vector fitting data.

After the SDD21 was extrapolated to DC, the group delay of the SDD21 was extracted. This task can be accomplished in several ways, using either time-frequency decompositions [39], [40], Hilbert transform [41], [42], [43], vector fitting [44], or DEFACT method [45]. The Hilbert transform method has been adopted because of its simplicity.

The transfer function SDD21 does not exhibit minimum phase. This is because of the delay embedded in the transfer function. Let T_d be the delay between the two ports of the system. Then SDD21 can be written as

$$S21(j\omega) = S21'(j\omega)e^{-j\omega T_d} \quad (1)$$

According to linear system theory [46] any stable system function can be represented as a product of a minimum phase function and an all-pass function, where an all-pass function is one whose magnitude is unity over the entire frequency range.

Therefore,

$$S21(j\omega) = S21_{\min}(j\omega)S21_{AP}(j\omega) \quad (2)$$

Comparing (1) and (2) noting that $e^{-j\omega T_d}$ has unity magnitude, it can be seen that if $S21(\omega)$ is separated into a product of a minimum phase function and an all-pass function, the all-pass function will represent the delay between the two ports. This separation can be performed using the Hilbert transform.

The Hilbert transform relates the magnitude and phase of a minimum phase function $H_{\min}(j\omega)$ through the equation

$$\arg[H_{\min}(j\omega)] = -\frac{1}{2\pi} P \int_{-\pi}^{\pi} \ln(|H_{\min}(j\theta)|) \cot\left(\frac{\omega-\theta}{2}\right) d\theta \quad (3)$$

where P is the Cauchy Principle value. Since an all-pass function was unity magnitude, the magnitude response of the minimum phase function $S21_{\min}(\omega)$ in Eqn(2) is the same as that of $S21(\omega)$. Therefore the port-to-port delay T_d embedded in the transfer function $S21(\omega)$ can be determined as follows

$$|S21_{\min}(j\omega)| = |S21_{AP}(j\omega)| \quad (4)$$

$$\arg[S21_{\min}(j\omega)] = -\frac{1}{2\pi} P \int_{-\pi}^{\pi} \ln(|S21(j\theta)|) \cot\left(\frac{\omega-\theta}{2}\right) d\theta \quad (5)$$

$$S21_{AP}(j\omega) = \frac{S21(j\omega)}{S21_{\min}(j\omega)} = e^{-j\omega T_d} \quad (6)$$

$$T_d = -\frac{\arg(S21_{AP}(j\omega))}{\omega} \quad (7)$$

The delay extracted above was then removed from the SDD21 response to apply delay causality. The delay causal condition for impulse response $h(t)$ is $h(t)=0$ when $t<t_d$, where t_d is the delay time. It is equivalent to consider $h(t+t_d)=0$ when $t<0$. The spectrum of $h(t+t_d)$, $H_d(\omega)$, can be obtained from the spectrum of $h(t)$, $H(\omega)$, by subtracting the delay phase

$$H_d(j\omega) = \exp(j\omega t_d) * H(j\omega) \quad (8)$$

To enforce delay causality, first, extrapolate $H_d(\omega)$ to Nyquist frequency, then enforce causality so that $H_d(\omega)$ is causal with respect to $t=0$. After the causal $h(t+td)$ is computed from $H_d(\omega)$, $h(t)$ is obtained by shifting $h(t+td)$ in time axis by td . The resulting $h(t)$ is then causal with respect to delay [49]. The impulse responses with and without forcing delay causality are compared in Figure 2.6. It can be seen that the key for delay causality is the optimal estimation of the time delay.

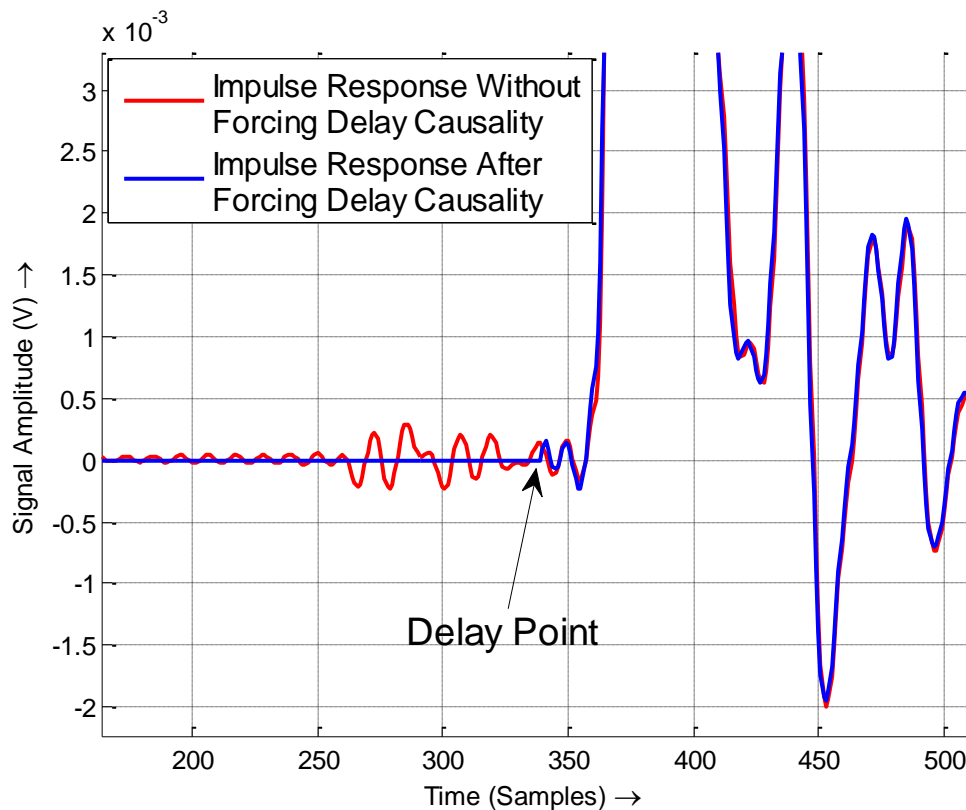


Figure 2.6. Impulse response obtained after forcing delay causality and without forcing delay causality.

The delay-removed SDD21 was then extrapolated to Nyquist frequency based on Sampling Theorem. In [49] a polynomial function up to 4th order was used to extend the

cut-off frequency to Nyquist frequency continuously. However, in the case shown here, the Nyquist frequency is too far away from the cut-off frequency, and therefore the quadric extrapolation cannot reveal the nature of the insertion loss transfer function SDD21.

Two extrapolation methods can be applied here. One is so called cosine extrapolation, which extrapolates the delay-removed $\text{real}(\text{SDD21})$ using an exponentially attenuated cosine wave. Figure 2.7 illustrates this method. The period of this cosine waveform is the average distance between the zero-crossing points of $\text{imag}(\text{SDD21})$. And the attenuation factor is chosen by intuition or can be obtained by curve fitting the envelope of the $\text{real}(\text{SDD21})$.

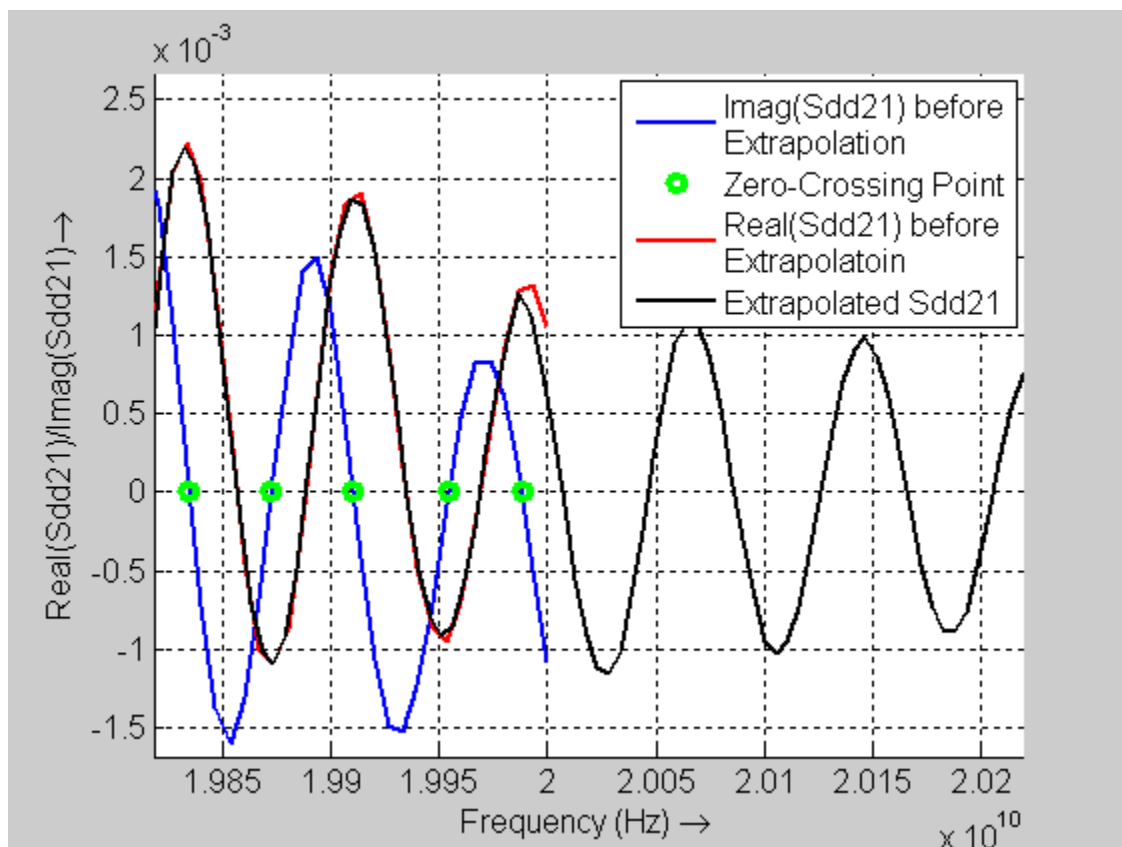


Figure 2.7. Find zero-crossing points and extrapolate the $\text{real}(\text{sdd21})$ to Nyquist frequency starting from the last zero-crossing point location.

Another extrapolation method is the so-called constant extrapolation, which extrapolates the delay-forced $\text{real}(\text{SDD21})$ using a constant value 0 as shown in Figure 2.8. Since the extrapolated SDD21 will be forced causality by Hilbert transform anyway, the discontinuity caused by this method will be no longer matter.

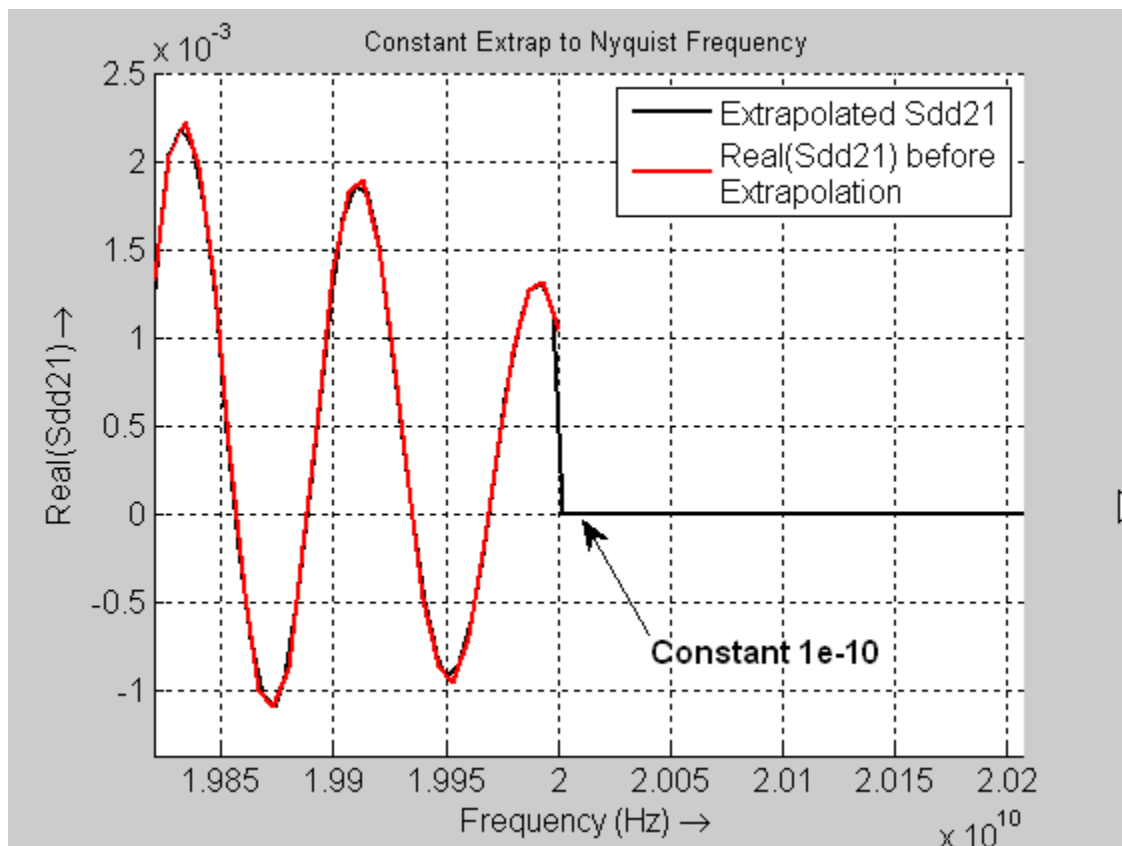


Figure 2.8. Extrapolate the $\text{real}(\text{Sdd21})$ to Nyquist frequency using a constant value.

A comparison of the influences on impulse response waveform from the two extrapolation methods is shown in Figure 2.9. These two methods give similar results, and therefore the constant extrapolation method is finally chosen because it is easier.

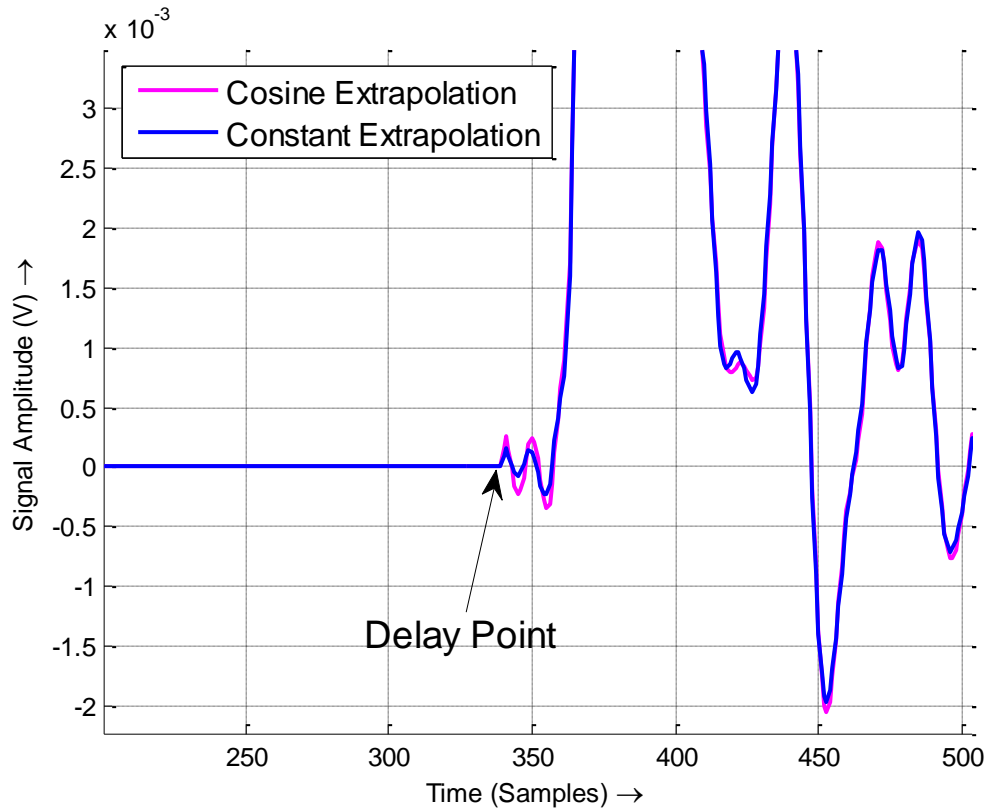


Figure 2.9. Comparison between cosine extrapolated and constant extrapolated impulse response.

After the extrapolation, causality was enforced on the extrapolated SDD21. A frequency response is causal when it complies with the dispersion relations. One equation of the dispersion relations in terms of the real and imaginary part of the frequency response is the Kramers-Kronig dispersion relations or Hilbert transform and holds if and only if the impulse response $h(t)$ vanishes for $t < 0$.

$$U(\omega) = \frac{1}{\pi} \int_{-\infty}^{\infty} \frac{V(\omega')}{\omega - \omega'} d\omega' \quad (9)$$

$$V(\omega) = -\frac{1}{\pi} \int_{-\infty}^{\infty} \frac{U(\omega')}{\omega - \omega'} d\omega' \quad (10)$$

The main limitation of standard Kramers-Kronig relations is their sensitivity to the high frequency data, which are not available in practice. The use of a generalized

formulation of dispersion relations named *dispersion relations with subtractions* has been proposed [50]-[54] to enforce causality using the band-limited tabulated frequency response with an accurate estimation of the error bound due to truncation error and discretization error.

In our approach, both MATLAB `hilbert.m` routine and the generalized dispersion relations method are considered. By applying real/imaginary Hilbert transform MATLAB routine on the real part of the delay-removed extrapolated SDD21, the original SDD21 is shown in Figure 2.10 and the final sound causal SDD21 is shown in Figure 2.11.

The causal SDD21 was applied IFFT to get an impulse response $h(t)$. The delay was added back to $h(t)$ by zero padding at the beginning as shown in Figure 2.12.

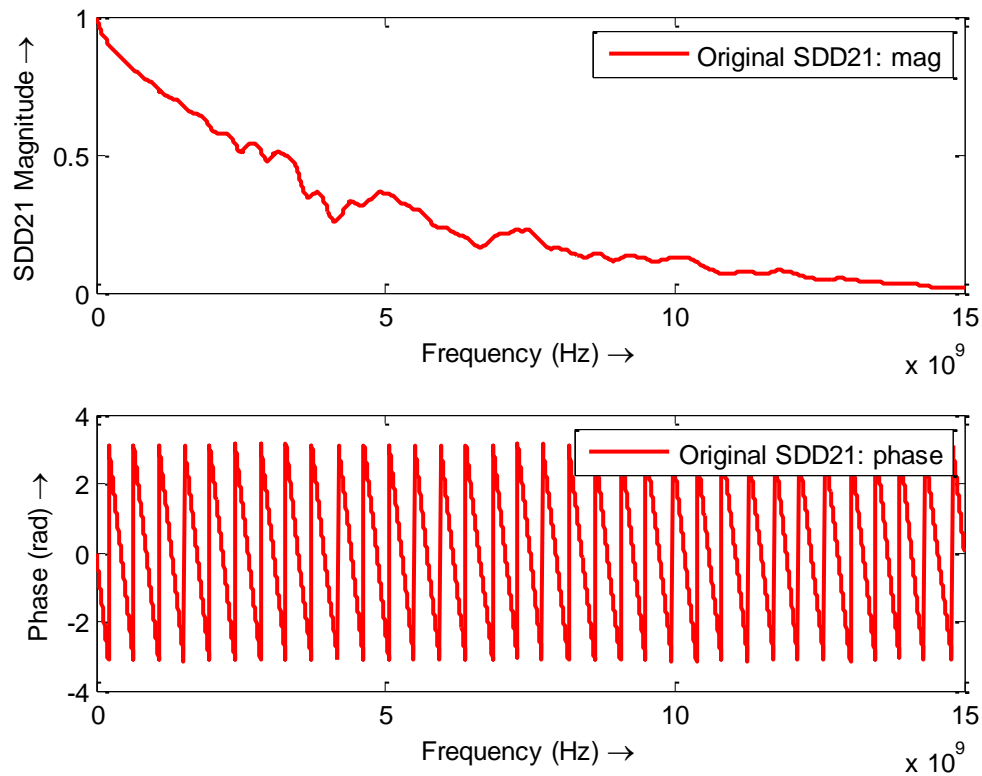


Figure 2.10. The original S-parameters.

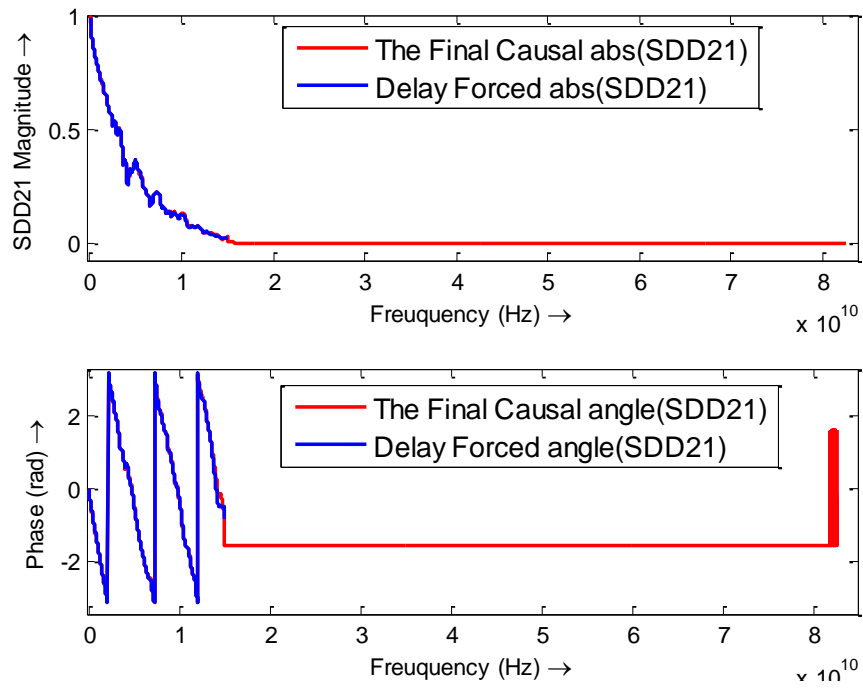


Figure 2.11. Comparison between the delay-forced SDD21 and the final causal SDD21.

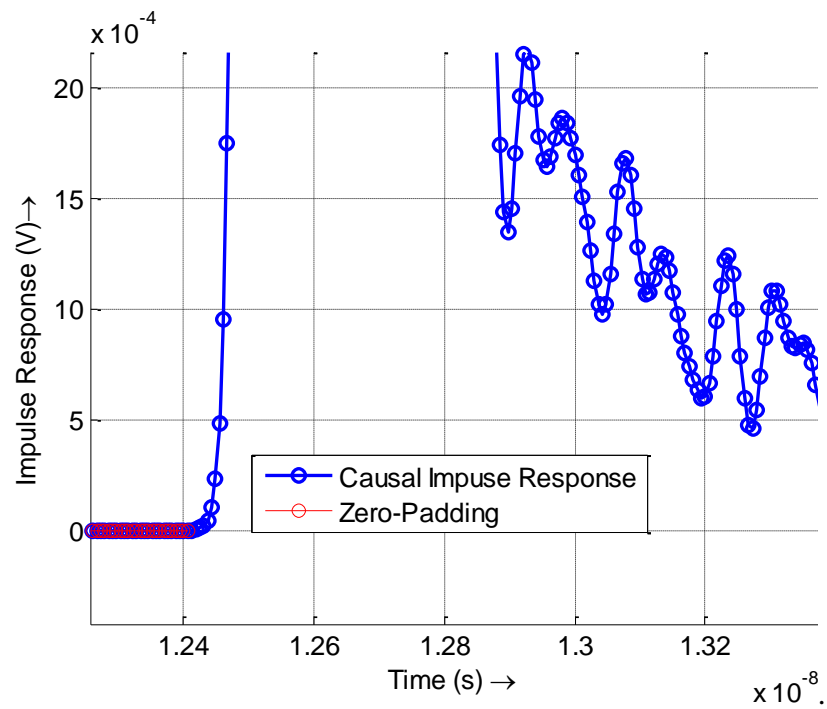


Figure 2.12. The causal impulse response waveform.

Then the $h(t)$ was convolved with an ideal step waveform to get a causal step response as shown in Figure 2.13.

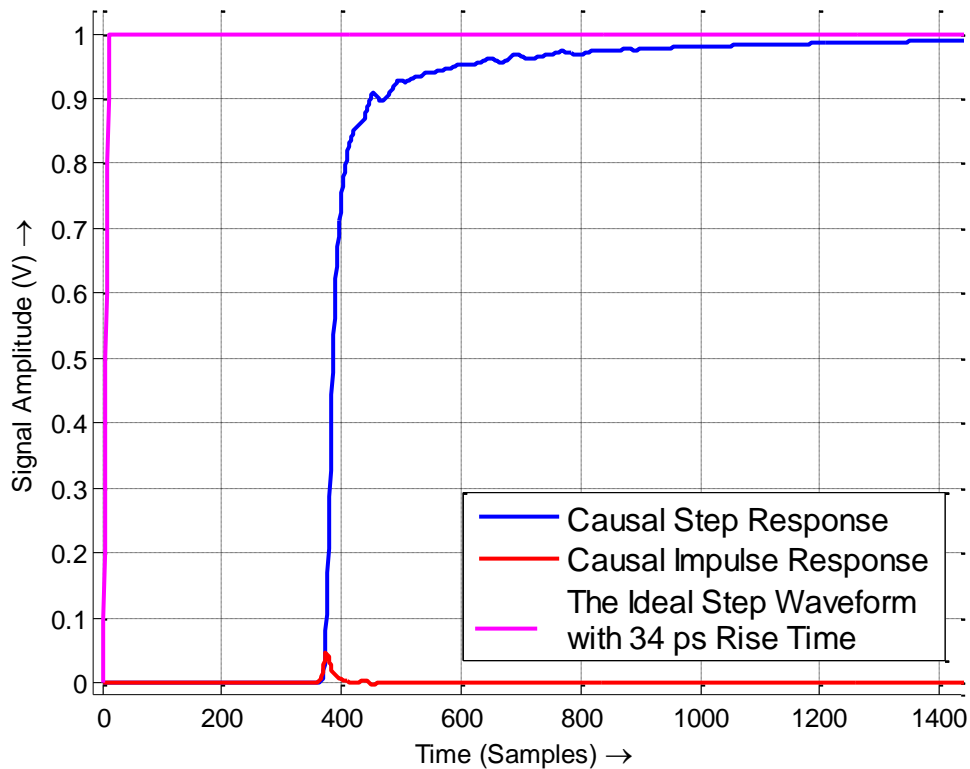


Figure 2.13. Comparison of step response and impulse response.

2.2.1.3 Shift and add step response. To calculate dWDP, the transition location of the PRBS9 pattern was found, and then the step response was superimposed to get the signal output waveform as shown in Figure 2.2.

A set of passive SFP+ copper cable was used to test both the frequency domain and time domain approach. In Figure 2.14, the waveform shown in red is generated by the frequency domain approach. The PRBS9 input waveform shown in blue is taken FFT and multiplied with the interpolated measured SDD21, and then an IFFT gives out the final waveform. The black dash curve is the result of the novel time domain method

proposed here. These two methods can give very close waveforms and dWDP values. A comparison of the two methods is shown in Table 2.1.

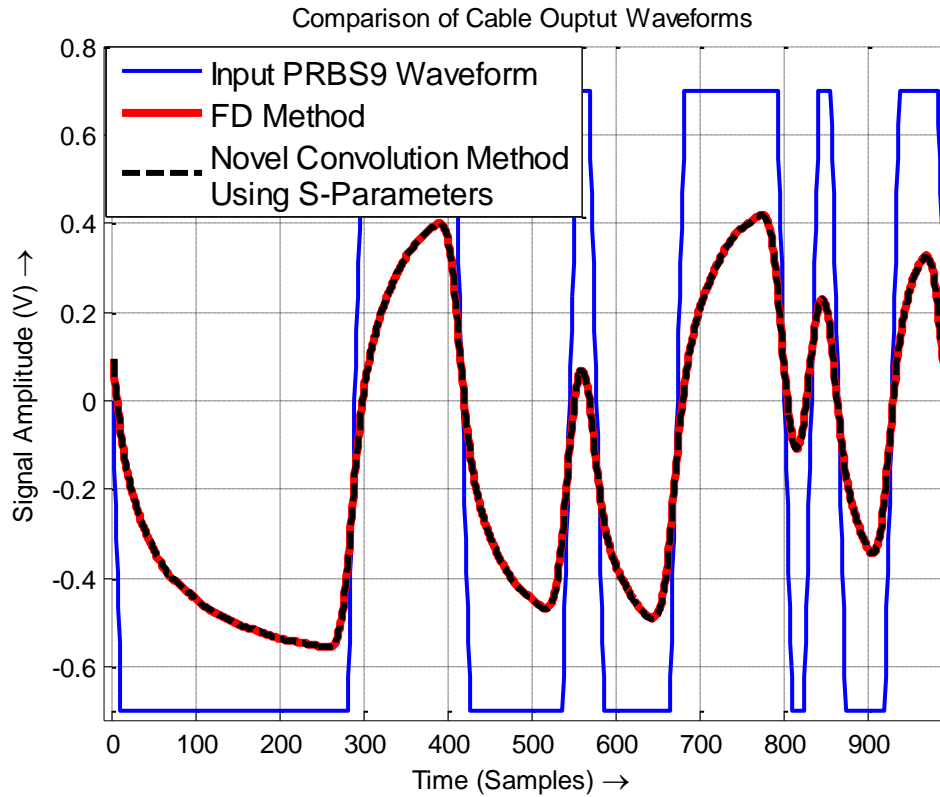


Figure 2.14. Comparison between frequency domain approach and time domain approach.

Table 2.1. Comparison of dWDP from different methods.

Method	dWDP value	Time Used
FD Approach	4.2048	0.66 s
TD Method using S-Parameters	4.2454	0.34 s

The two methods give close results, but the time domain approach only uses half the time. Although the dWDP calculation does not require longer sequence but PRBS9, an interesting test was performed to show the time and memory efficiency of the time domain method. The same S-parameters were used for both FD approach and TD approach, data patterns up to PRBS15 was used. All calculations were run in MATLAB 7.8.0 (R2009a) on a laptop with a 2.0 GHz processor, 2.0 GB memory, and Windows 7 operating system. The results are compared below in Table 2.2.

Table 2.2. Comparison of FD & TD time consumption.

Signal Pattern	Methods Used	
	FD Method	Novel Convolution Method
PRBS-9	0.66 s	0.34 s
PRBS-11	3.44 s	1.69 s
PRBS-13	74.8 s	7.20 s
PRBS-15	394.7 s	18.2 s

As the data sequence becomes longer, the FD method uses much longer time than the novel TD method.

2.2.2. NEXT. The Near End Crosstalk (NEXT) is defined as the RMS voltage measured by a free running oscilloscope in a bandwidth of 12 GHz when a PRBS31 NEXT source is injected. The PRBS9 waveform can be used in the FD method to approximate the NEXT voltage. Also a statistical analysis is available to estimate the NEXT using the time domain pulse response.

2.2.2.1 Statistical estimation using pulse response. The Pseudo-Random-Binary-Sequence (PRBS) signal is generated factitiously for simulating a naturally random sequence which has 50% probability of '1' bits and 50% probability of '0' bits.

The NEXT waveform can be considered as a pulse response shifted by one bit each time and superimposed according to the PRBS31 transitions.

In the case that a total of m samples $\{x_1, x_2, \dots, x_m\}$, the RMS value (NEXT) is calculated by

$$\text{NEXT} = x_{rms} = \sqrt{\frac{x_1^2 + x_2^2 + \dots + x_m^2}{m}}, m = n * L \quad (11)$$

where L is the number of bits in a sequence, and n is the samples per bit. Here L is $2^{31}-1$, and n we consider it as 32 samples/bit.

Similar with the statistical eye analysis, the total m samples are overlapped within one UI. Therefore the total m samples are divided into n groups. The samples within each group have a distribution depending on the location of the groups, as shown in Figure 2.15.

Apply Central Limit Theorem
on each groups of samples

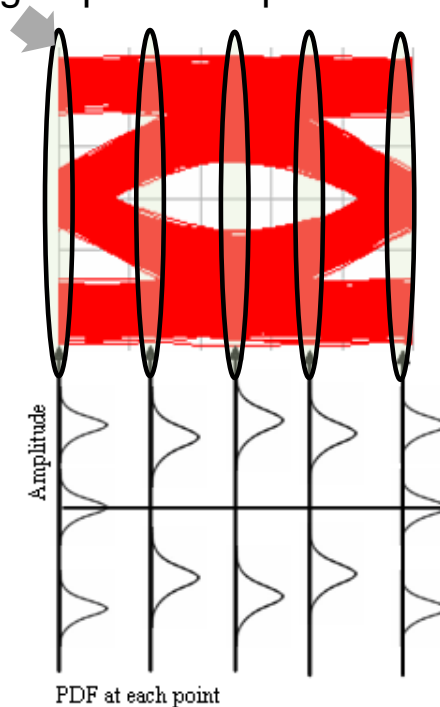


Figure 2.15. Distributions of random variables denoting different groups of samples.

$$\begin{aligned}
\text{NEXT} &= \sqrt{\frac{[(x_1^2 + x_{1+n}^2 + x_{1+2n}^2 + \dots + x_{1+(L-1)n}^2) + \\
&\quad (x_2^2 + x_{2+n}^2 + x_{2+2n}^2 + \dots + x_{2+(L-1)n}^2) + \\
&\quad \dots + \\
&\quad (x_n^2 + x_{n+n}^2 + x_{n+2n}^2 + \dots + x_{n+(L-1)n}^2)]}{nL}} \\
&= \sqrt{\frac{S_1 + S_2 + \dots + S_n}{n}}
\end{aligned} \tag{12}$$

where

$$\begin{aligned}
S_1 &= (X_1 + X_{1+n} + X_{1+2n} + \dots + X_{1+(L-1)n}) / L \\
S_2 &= (X_2 + X_{2+n} + X_{2+2n} + \dots + X_{2+(L-1)n}) / L \\
&\dots \\
S_n &= (X_n + X_{n+n} + X_{n+2n} + \dots + X_{n+(L-1)n}) / L
\end{aligned} \tag{13}$$

and

X_i denotes the random variable x_i^2 in Eqn 11.

Within each group, for example, in the 1st group, all the random variables $X_1, X_{1+n}, X_{1+2n}, \dots, X_{1+(L-1)n}$ satisfy:

- a. Sufficiently large number of random variables, i.e., in total L samples.
- b. Identical distribution, i.e., at the same location of the eye diagram.
- c. Weak dependence, i.e., only samples from adjacent bits influence each other.

The Central Limit Theorem [55] can be applied on each group of samples, and the random variables S_1, S_2, \dots, S_n converge to normal distribution.

$$\begin{aligned}
Z_1 &= \frac{S_1 - \mu_1}{\sigma_1 / \sqrt{L}} = \frac{S_1 - E(X_1)}{\sigma_1 / \sqrt{L}} \sim N(0,1) \\
Z_2 &= \frac{S_2 - \mu_2}{\sigma_2 / \sqrt{L}} = \frac{S_2 - E(X_2)}{\sigma_2 / \sqrt{L}} \sim N(0,1) \\
&\dots \\
Z_n &= \frac{S_n - \mu_n}{\sigma_n / \sqrt{L}} = \frac{S_n - E(X_n)}{\sigma_n / \sqrt{L}} \sim N(0,1)
\end{aligned} \tag{14}$$

The expectation and variance of random variables S_1, S_2, \dots, S_n can then be obtained.

$$\begin{aligned}
E(S_1) &= E(X_1), \quad \text{var}(S_1) = [\text{var}(X_1)]^2 / L \ll 1 \\
E(S_2) &= E(X_2), \quad \text{var}(S_2) = [\text{var}(X_2)]^2 / L \ll 1 \\
&\dots \\
E(S_n) &= E(X_n), \quad \text{var}(S_n) = [\text{var}(X_n)]^2 / L \ll 1
\end{aligned} \tag{15}$$

Define a new random variable \overline{S}_n as the average of S_1, S_2, \dots, S_n , which also equals to NEXT². The expectation and variance of \overline{S}_n can be derived.

$$\begin{aligned}
\overline{S}_n &= \frac{S_1 + S_2 + \dots + S_n}{n} \\
E(\overline{S}_n) &= \frac{\sum_{i=1}^n E(S_i)}{n} = \frac{\sum_{i=1}^n E(X_i)}{n} \\
\text{var}(\overline{S}_n) &= \frac{1}{n^2} \left[\sum_{i=1}^n \text{var}(S_i) + 2 \sum_{i < j} \text{Cov}(S_i, S_j) \right] \\
&\leq \frac{1}{n^2} \left[\sum_{i=1}^n \text{var}(S_i) + 2 \sum_{i < j} \sqrt{\text{var}(S_i) \text{var}(S_j)} \right] \\
&\ll \frac{1}{n^2}
\end{aligned} \tag{16}$$

The Cauchy–Schwarz inequality $|Cov(S_i, S_j)| \leq \sqrt{\text{var}(S_i) \text{var}(S_j)}$ [56] and Eqn (15) were used above to get the upper bound for $\text{var}(\overline{S_n})$.

Since $\overline{S_n} = \text{NEXT}^2$, $\text{var}(\text{NEXT}) = \text{var}(\sqrt{\overline{S_n}})$ can be also considered as a value which is much smaller than $\frac{1}{n^2}$.

$$\text{var}(\text{NEXT}) = \text{var}(\sqrt{\overline{S_n}}) \ll \frac{1}{n^2} \quad (17)$$

After the derivations above, the expectation of NEXT can be written as:

$$\begin{aligned} E(\text{NEXT}) &= \sqrt{[E(\text{NEXT})]^2} \\ &= \sqrt{E(\text{NEXT}^2) - \text{var}(\text{NEXT})} \\ &= \sqrt{E(\overline{S_n}) - \text{var}(\sqrt{\overline{S_n}})} \\ &\approx \sqrt{\frac{\sum_{i=1}^n E(X_i)}{n}} \end{aligned} \quad (18)$$

Now the only task left is to calculate $E(X_i)$, which can be derived from probability analysis. Random variable X_i denotes the square of the random variable x_i . As shown in Figure 2.16, the random variable x_i is the superimposition of point A, B, C, D ...

Define the pulse response as $r(n)$, and $R_{i,j}$ means the random variable have the distribution of 50% $r(i+(j-1)*n)$ and 50% of $-r(i+(j-1)*n)$, where the n means the samples per bit of the pulse response $r(n)$, “ i ” means the samples group index, and “ j ” means the bit index.

$$\begin{aligned}
x_i &= R_i + R_{i+n} + R_{i+2n} \dots + R_{i+(M-1)n} \\
x_i^2 &= (R_i + R_{i+n} + R_{i+2n} \dots + R_{i+(M-1)n})^2 \\
&= R_i^2 + R_{i+n}^2 + R_{i+2n}^2 \dots + R_{i+(M-1)n}^2 + \sum_{\substack{j,k=0 \\ j \neq k}}^{M-1} R_{i+j*n} R_{i+k*n} \\
E(x_i^2) &= E(R_i^2 + R_{i+n}^2 + R_{i+2n}^2 \dots + R_{i+(M-1)n}^2 + \sum_{\substack{j,k=0 \\ j \neq k}}^{M-1} R_{i+j*n} R_{i+k*n}) \\
&= \sum_{j=0}^{M-1} E(R_{i+j*n}^2) + \sum_{\substack{j,k=0 \\ j \neq k}}^{M-1} E(R_{i+j*n} R_{i+k*n}) \\
&= \sum_{j=0}^{M-1} [0.5 \times (+r_{i+j*n}^2) + 0.5 \times (-r_{i+j*n}^2)] + 0 \\
&= \sum_{j=1}^{M-1} r_{i+j*n}^2
\end{aligned} \tag{19}$$

where, M means the total bit number of the pulse response. R_{i+j*n} and R_{i+k*n} are independent. So NEXT voltage can be finally simplified from Eqn (18) and Eqn(19) as:

$$E(\text{NEXT}) \approx \sqrt{\frac{\sum_{i=1}^n \sum_{j=1}^M r(i+(j-1)M)^2}{n}} = \sqrt{\frac{\sum_{k=1}^{n*M} r(k)^2}{n}} \tag{20}$$

This equation only requires the pulse response to estimate the NEXT. And it holds when L is sufficiently large, and M is long enough for the pulse response to vanish. In this case, L is $2^{31}-1$ and is large enough to ignore the effect of variance effect. This is a very useful estimation equation for real cable measurement. All information needed is a pulse response of the NEXT. The pulse response can be obtained by shifting the step response by one bit and subtracting itself. Therefore a reasonable step response that represents the NEXT transfer function is of great importance in estimating the correct NEXT value.

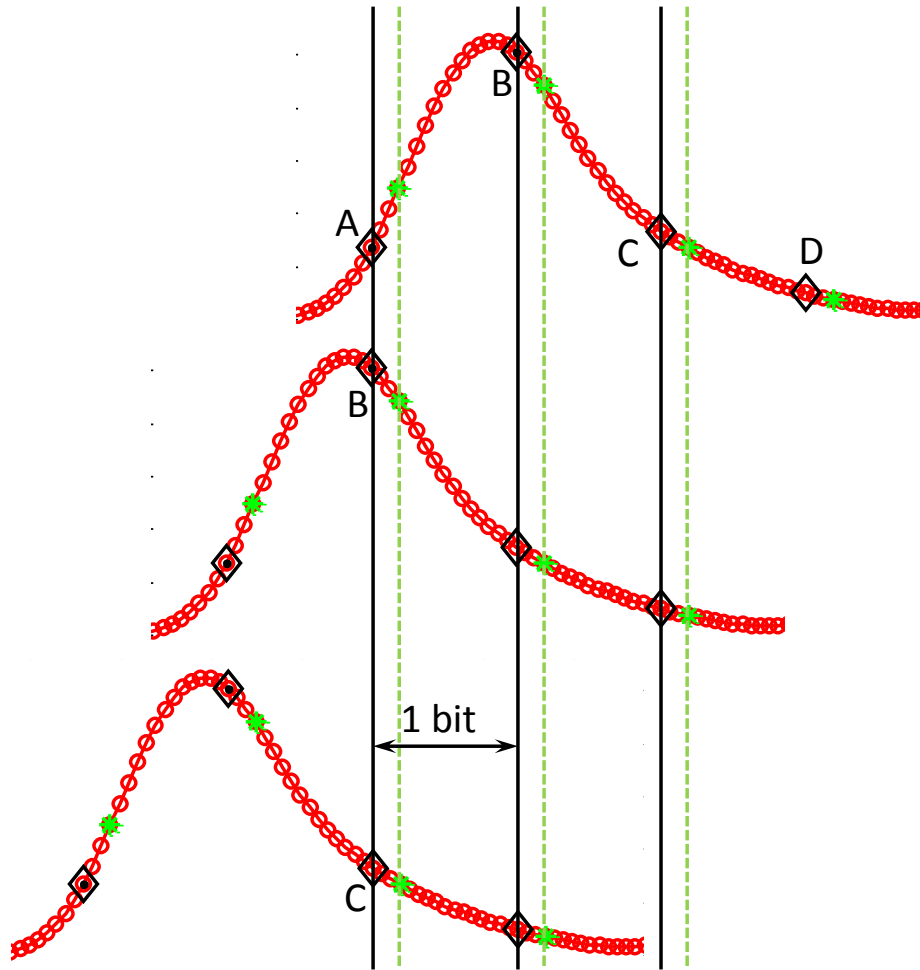


Figure 2.16. Illustration of pulse response shifting and superimposition.

2.2.2.2 Get reasonable pulse response. The pulse response can be obtained by shifting the step response by one bit and subtracting itself. Therefore a reasonable step response that represents the NEXT transfer function is of great importance in estimating the correct NEXT value. The NEXT step response can be measured by a TDR instrument, or a similar process in dWDP calculation works as well. The NEXT transfer function SDD21 is processed like in 2.2.1.2, only except the extrapolation of S-parameters is more complicated and no delay is forced, since we consider it as “Near End”.

The raw SDD21 is shown in Figure 2.17. The quadratic extrapolation fails because the Nyquist frequency is too far away from the cut-off frequency. The constant 0

extrapolation is not suitable either since the high frequency components of NEXT SDD21 does not diminish like the insertion loss transfer function. The method chosen here is to use a constant value to approximate the mean power of S-parameters beyond the cut-off frequency. The extrapolated SDD21 is shown in Figure 2.18.

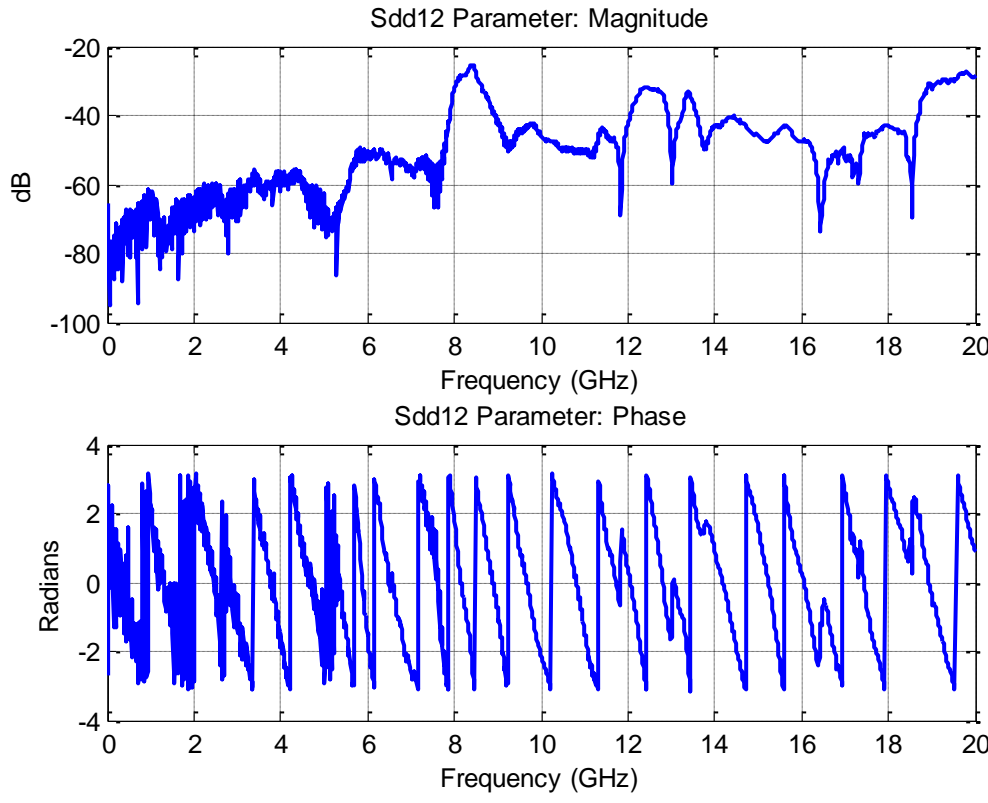


Figure 2.17. Original SDD21 of NEXT S-parameters.

There is a little tricky in extrapolating the NEXT S-parameters. Since there is no clear trend how the SDD21 of NEXT is, unlike the SDD21 of cable transferring, the estimation of higher frequency component becomes a guess. Usually a manipulation is just small constant value estimation for ignore the high frequency component.

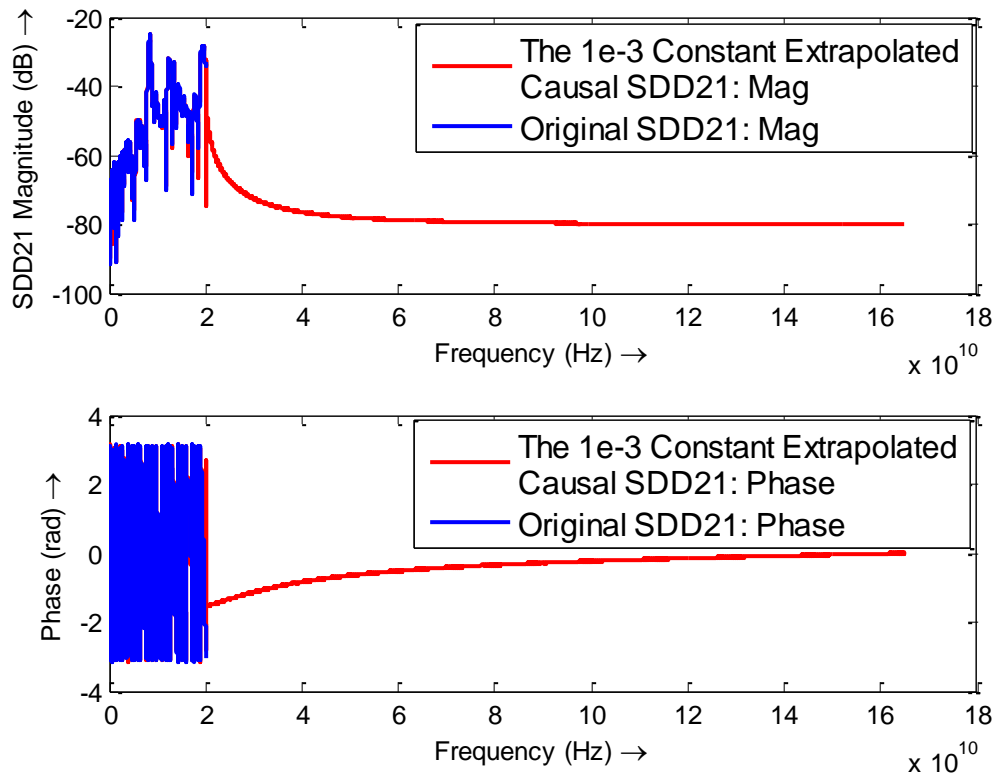


Figure 2.18. 1e-3 constant extrapolation on SDD21 of NEXT S-parameters.

A pulse response obtained after constant extrapolation of 1e-3 is shown in Figure 2.19. The NEXT value is 1.2639 mV from TD method and 1.2719 mV from FD PRBS9 approximation as shown in Table 2.5 of Section 2.4.2. The results are reasonable since the high frequency components of SDD21 are underestimated in TD method.

In real measurement, the NEXT is easily changed by the noise level. In the standard, the NEXT is defined as the RMS voltage measured by a free running oscilloscope in a bandwidth of 12 GHz when a PRBS31 NEXT source is injected. In this case, if the noise model is considered as a Gaussian white noise one, the mean value of the noise is zero and can be approximately ignored.

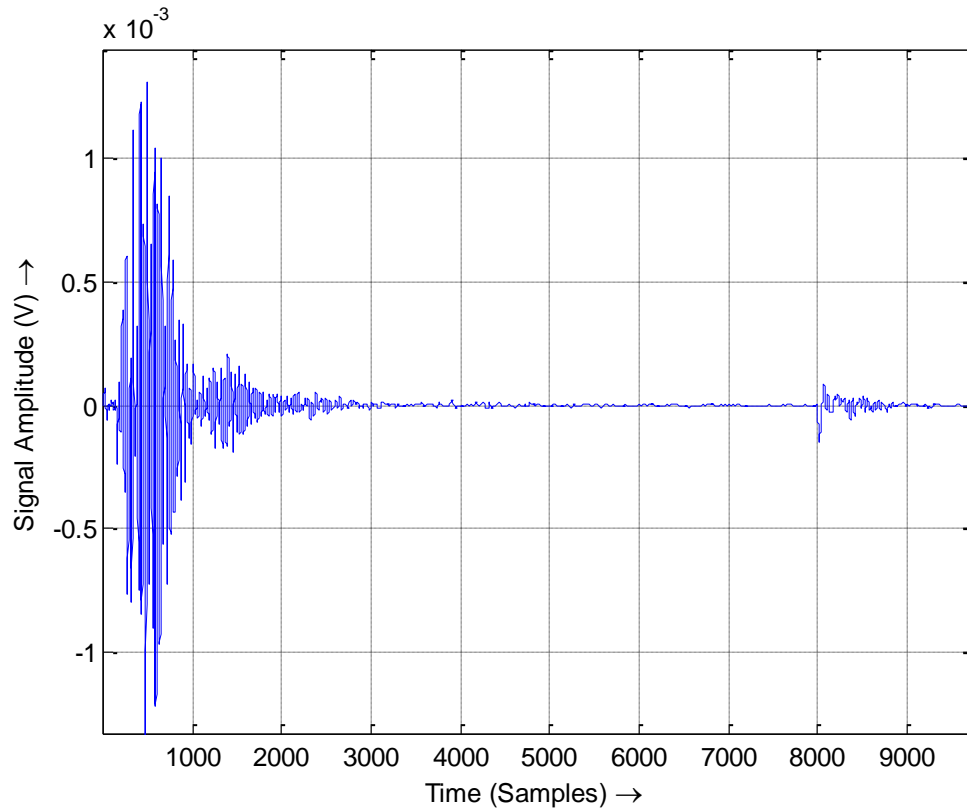


Figure 2.19. Pulse response after constant extrapolation of $1e-3$ on SDD21 of NEXT.

2.2.2.3 Verification by statistical numerical simulation. Having the same thoughts as in 2.2.2.1, the pulse response is shifted by one UI and superimposed. However we do not use the Central Limit Theorem approximation, but apply a random $(-1,1)$ sequence to our pulse response, and get all the possible voltage values based on this random sequence, then the NEXT can be calculated by the root mean square of all possible voltage values.

Below are the steps for statistical numerical simulation.

1. Generate random sequence of -1 and 1, by a MATLAB code:

$$\text{Sequence} = (\text{randi}(2,[I, \text{BLen}]) - 1.5) * 2;$$

where, $BLen$ is the random sequence length. According to the NEXT definition, $BLen$ should be $2^{31}-1$. But, MATLAB has a length limitation of about 2^{27} . Actually in this numerical simulation, usually 2^{15} is good enough.

- Shift ONE sample and Get All combinations as shown in Figure 2.20.

The cursor number here means 'L'.

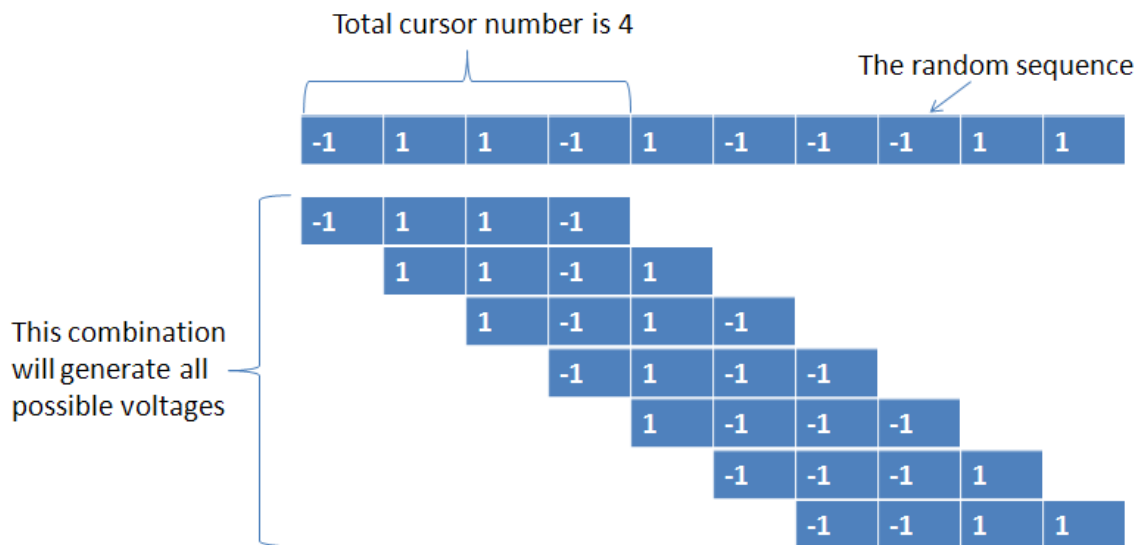


Figure 2.20. Illustration of statistical numerical simulation.

- Get all possible values

The method getting all possible combinations is shown in Figure 2.21.

- RMS the values

Then just get the rms value of all the Voltages in the results.

- Repeat Step 1~4 by 1000 times for consistency.

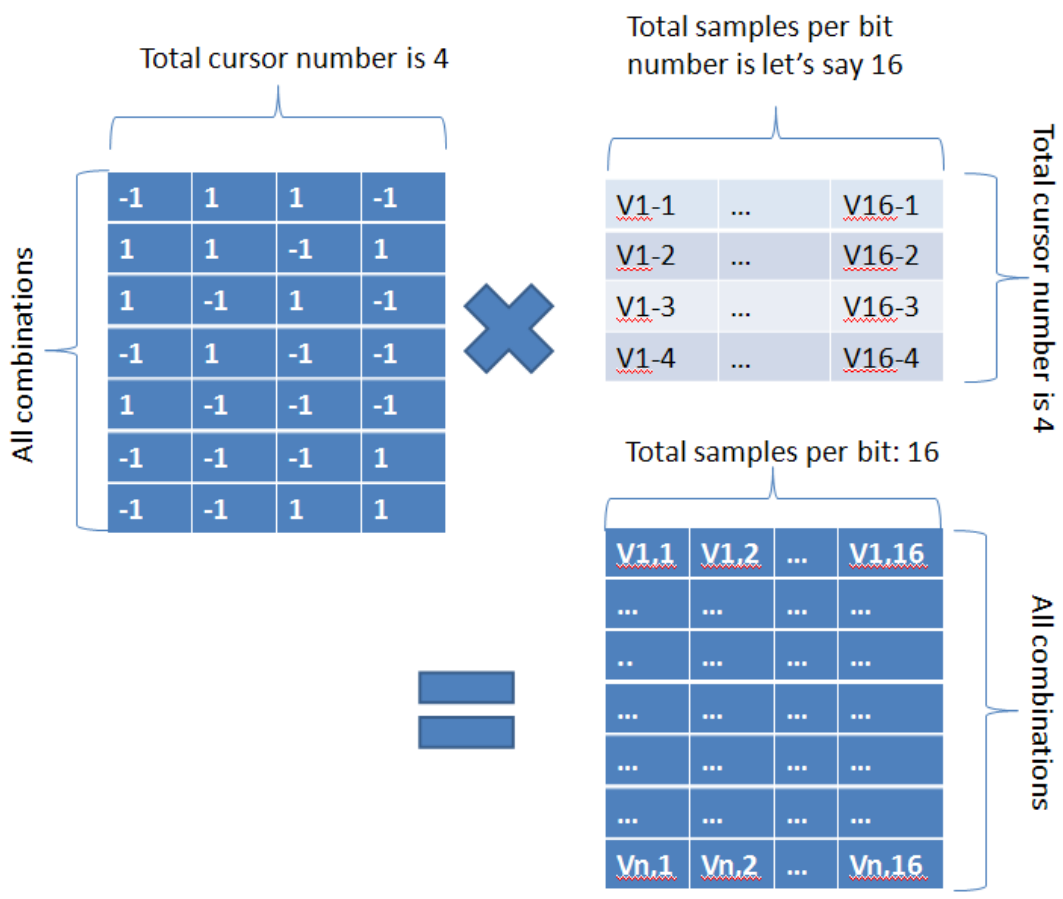


Figure 2.21. Illustration of how to get all possible combinations.

The results are compared below in Table 2.3, which verifies the derivation in 2.2.2.1 is correct.

Table 2.3. Comparison of NEXT value from multiple numerical simulations.

Statistical Equation (mV)	Numerical Repeat #1 (mV)	Numerical Repeat #2 (mV)	Numerical Repeat #3 (mV)	Numerical Repeat #4 (mV)	Numerical Repeat #5 (mV)
1.2639	1.2413	1.2993	1.2674	1.2734	1.2739

2.2.3. Vcm. The common mode voltage at any time is the average of signal+ and signal- at that time. The RMS AC common mode voltage (Vcm) can be calculated using the same method as NEXT, only except the Vcm sources include both crosstalk and insertion loss transfer function, and SDC21 is processed here instead of SDD21.

2.2.4. L and VCR. VMA Loss (L) is defined as:

$$L(dBe) = 20 * \log_{10} \left(\frac{VMA_i}{VMA_o} \right)$$

where VMA_i and VMA_o is an output parameter of the WDP code in SFF-8431 Appendix G.

VMA/2 to crosstalk ratio (VCR) can be calculated as:

$$VCR(dBe) = 20 * \log_{10} \left(\frac{VMA_{min}}{2 * NEXT * (1 + C)} \right) - L$$

where

$$VMN_{min} = 300 \text{ mV when } VMA_{max} = 700 \text{ mV}$$

$$C = 0.3 \times 10^{\left(\frac{-2L}{20} \right)}$$

2.2.5. SDD_{xx} and SCC_{xx}. If using S-parameters, the SDD_{xx} and SCC_{xx} are directly measured by VNA.

The SDD_{xx} mask is given by equation:

$$SDD_{xx}(dB) = -12 + 2 \times \text{SQRT}(f), \text{ with } f \text{ in GHz, and } 0.01 < f < 4.1.$$

$$SDD_{xx}(dB) = -6.3 + 13 \times \log_{10}(f/5.5), \text{ with } f \text{ in GHz, and } 4.1 < f < 11.1.$$

The SCC_{xx} mask is given by equation:

$$SCC_{xx}(dB) < -7 + 1.6 \times f, \text{ with } f \text{ in GHz, and } 0.01 < f < 2.5.$$

$$SCC_{xx}(dB) = -3, \text{ when } 2.5 < f < 11.1 \text{ GHz.}$$

2.3. TIME DOMAIN METHODOLOGY USING TDT MEASUREMENT

From the discussion in Section 2.2, the essence of the novel time domain methodology is to get a causal, reasonable, and correct step response. The step response can be directly measured by the TDR instrument.

2.3.1. dWDP. dWDP is calculated by subtracting WDPi from WDPo.

2.3.1.1 Measure the step response by TDR instrument. Figure 2.22 shows the measured differential step response of a set of passive SFP+ copper cable assembly and the differential open calibration reference.

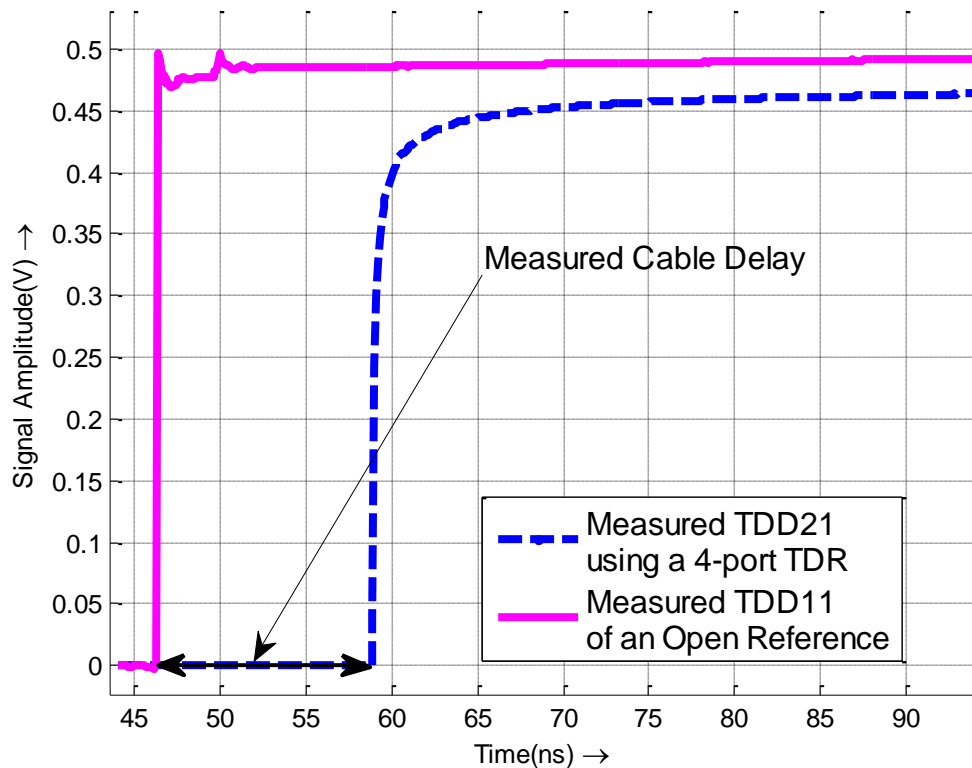


Figure 2.22. Measured TDD21 and cable delay.

When measuring the differential step response, several aspects influence the final dWDP results.

- De-skew of differential TDR signal is needed.

- Adequate average should be used to increase SNR of the step response.
- The number of samples per bit plays a role in dWDP calculation [29]; therefore adequate resolution is preferred even this may lead into longer record length.
- The rise/fall time is also important, a target 20~80% rising edge of 34 ps is required according to the SFF-8431 standard. So a rise time filter should be used if the TDR rise time is less than 34 ps.
- Another parameter is the time span of the TDT waveform. Usually a span long enough is chosen to ensure the step response goes to a steady state; however a too long time span is useless but only introduces extra noise since there is little information in a steady state. In some cases, the channel under test is AC coupling, which means there is no steady state. Therefore, a proper span chose is even more important.

2.3.1.2 Shift and add step response. The measured TDD21 step response waveform was shifted and added together to generate the PRBS9 output waveform. And an auto-correlation adjustment on the waveform was applied for better alignment with the input PRBS9 signal. An output waveform from the measured TDD21 step response is shown in Figure 2.23.

2.3.1.3 Take the optimized TDR/TDT measurement. Several TDT step response measurements with different time span were taken for comparing the effect of different span on dWDP calculation. For better comparison, other parameters are set as:

- The differential TDR signal is de-skewed.
- Average is set to 1000 times.
- The resolution is set to 2 ps constant, and 32 samples/bit is used for interpolation in dWDP calculation.
- The rise time is set to approximately 34 ps.
- TDR: Tektronix DSA8200
Scope: Tektronix DSA71254B

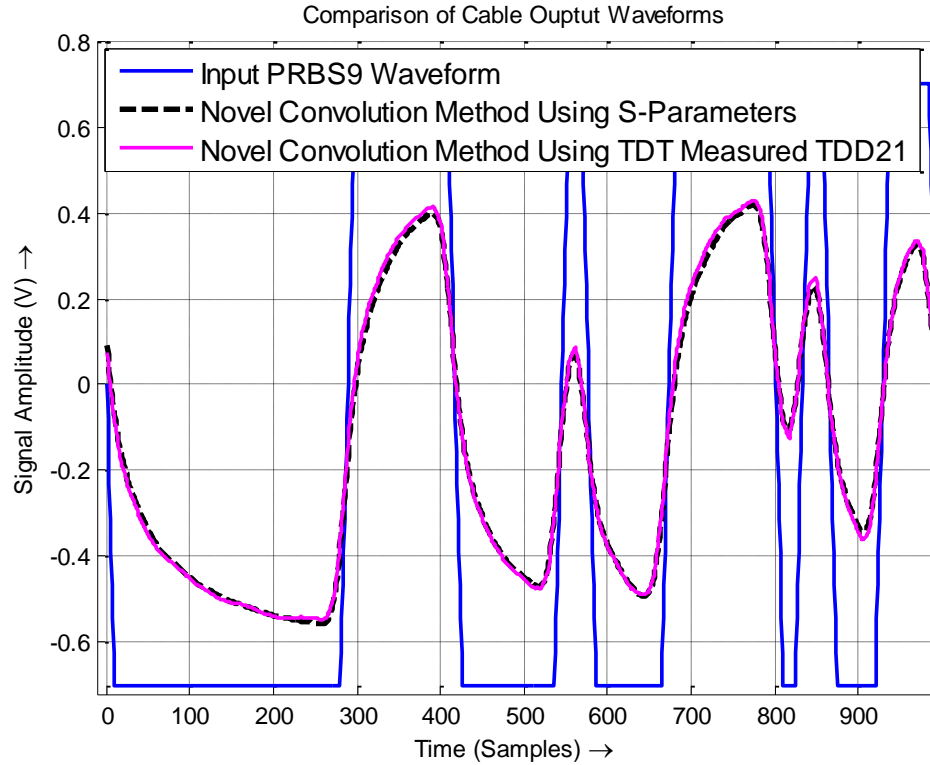


Figure 2.23. Comparison between TD approach using SDD21 and measured TDD21.

2.3.2. NEXT. The Near End Crosstalk (NEXT) is defined as the RMS voltage measured by a free running oscilloscope in a bandwidth of 12 GHz when a PRBS31 NEXT source is injected.

2.3.2.1 Measure the step response by TDR instrument. Figure 2.24 shows the measured differential NEXT step response of a set of passive SFP+ copper cable assembly. 1000 times average was used to increase the SNR.

2.3.2.2 Apply statistical estimation using pulse response. The pulse response was obtained from measured NEXT step response, and the statistical estimation was applied on the pulse response. The TDR 20~80% rise time is about 12 ps, and the differential TDR source amplitude is about 0.5 V. Taking these into account, comparison of the TDR results with S-Parameters results are shown in Table 2.5 of Section 2.4.2.

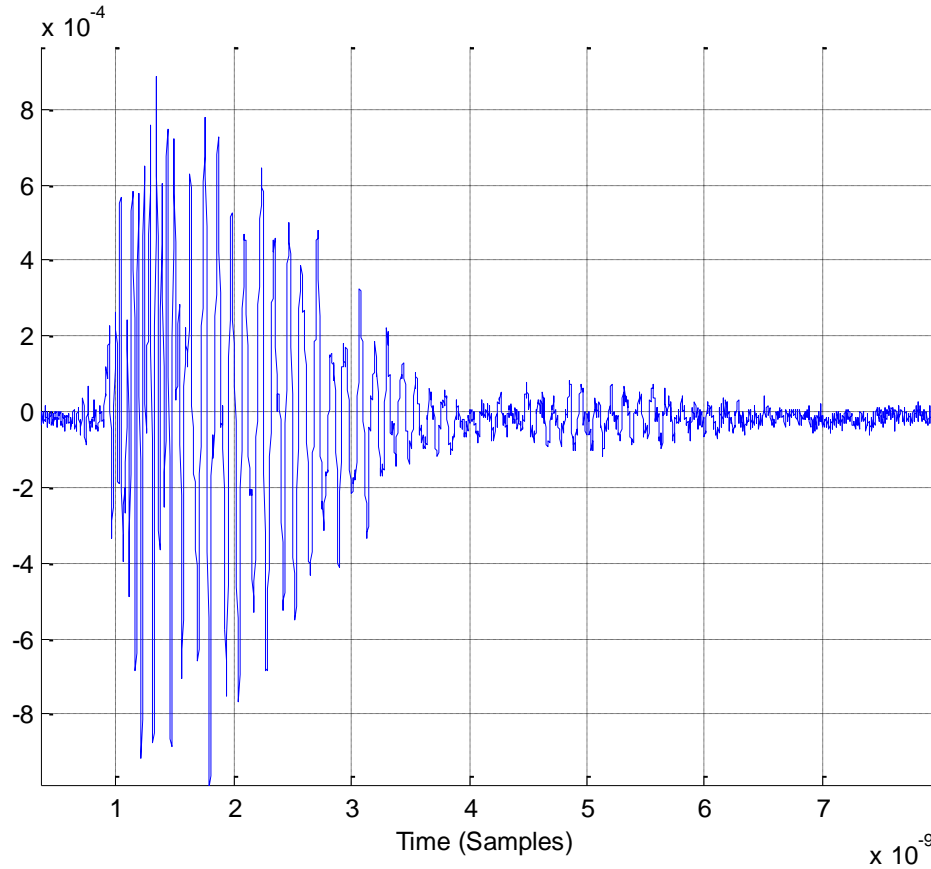


Figure 2.24. Measured TDD21 step response of NEXT.

2.3.3. Vcm. The similar TDR measurement like NEXT is used here for measuring Vcm.

2.3.4. L and VCR. The procedure is the same as Section 2.2.4.

2.3.5. SDDxx and SCCxx. The extraction of S-parameters from transient response has been developed over years. The most success method may be the Generalized Pencil-Of-Function Method (GPOF) [57]-[60]. The extraction of SDDxx and SCCxx is not discussed here.

2.4. VALIDATION OF NOVEL TIME DOMAIN METHODOLOGY

Using the same set of cable assembly, measurements based on SFF-8431 Appendix E were taken for validating the novel time domain methodology.

The cable set here is Gore, 3 meters long.

2.4.1. dWDP. A measurement based on the SFF-8431 standard [27] was performed to validate the proposed method. A host compliance board (HCB) is used to measure WDPi. The WDPi should be adjusted to a target value of 2.4 dB by changing the pre-emphasis taps of the compliance signal generator. The cable was then connected to the compliance signal generator and an oscilloscope via two MCBs. The cable output waveform was recorded to get WDPo, and then dWDP is calculated by subtracting WDPi from WDPo.

Different pre-emphasis taps combinations were tried to calculate dWDP. It shows that all combinations give a similar dWDP although the WDPi's and WDPo's may be quite different. This means the proposed method can be used without pre-emphasis. The measurement results comparison of different pre-emphasis combinations is shown in Table 2.4.

Table 2.4. Comparison of dWDP measurement results from different pre-emphasis.

	WDPi	WDPo	dWDP
#1	1.7244	5.7004	3.9760
#2	1.9634	5.9612	3.9978
#3 (As in Standard)	2.3969	6.3911	3.9942
#4	2.5661	6.5817	4.0156
#5	2.9993	6.9515	3.9522
No Pre-Emphasis	4.9966	9.0876	4.0910

2.4.2. NEXT. The NEXT measurement is performed using BERT Scope for NEXT source and Agilent DCA-J 86100C to observe. The crosstalk source Vp-p is set to 700 mV as shown in Figure 2.25, the data pattern is PRBS31, and the bit rate is 10.3125 Gbps.

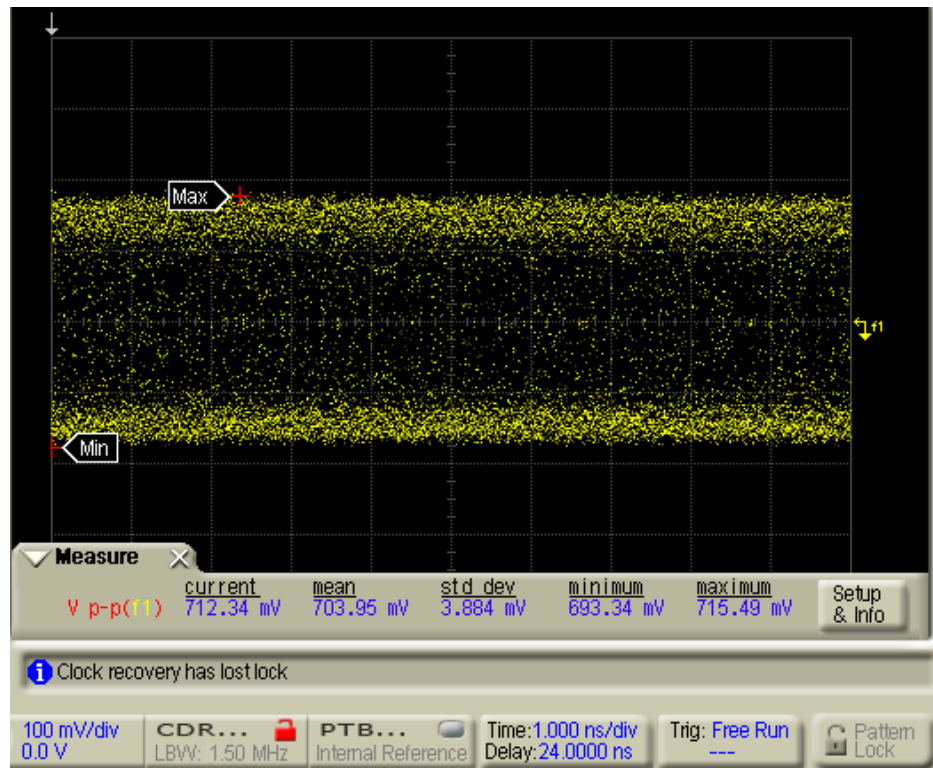


Figure 2.25. NEXT Source voltage amplitude (p-p) is 700 mV.

The measured NEXT value is scaled by $V_{pp}=1000$ mV and the value is shown in Table 2.5 as $0.9218/0.7 = 1.3168$ mV, which means the novel time domain method, can be used for NEXT evaluation. The measurement screen shot is shown in Figure 2.26.

Table 2.5. Comparison of NEXT evaluation from three methods.

Condition: Vpp=1V	12 ps	34 ps
FD Method PRBS9 Approximation	1.9362 mV	1.2719 mV
TD Method Using S-Para	$3.8577/2 = 1.9289$ mV	$2.5278/2 = 1.2639$ mV
TDT Measurement	$1.8972*2/2 = 1.8972$ mV	---
BERT Scope Measurement	---	$0.9218/0.7 = 1.3168$ mV

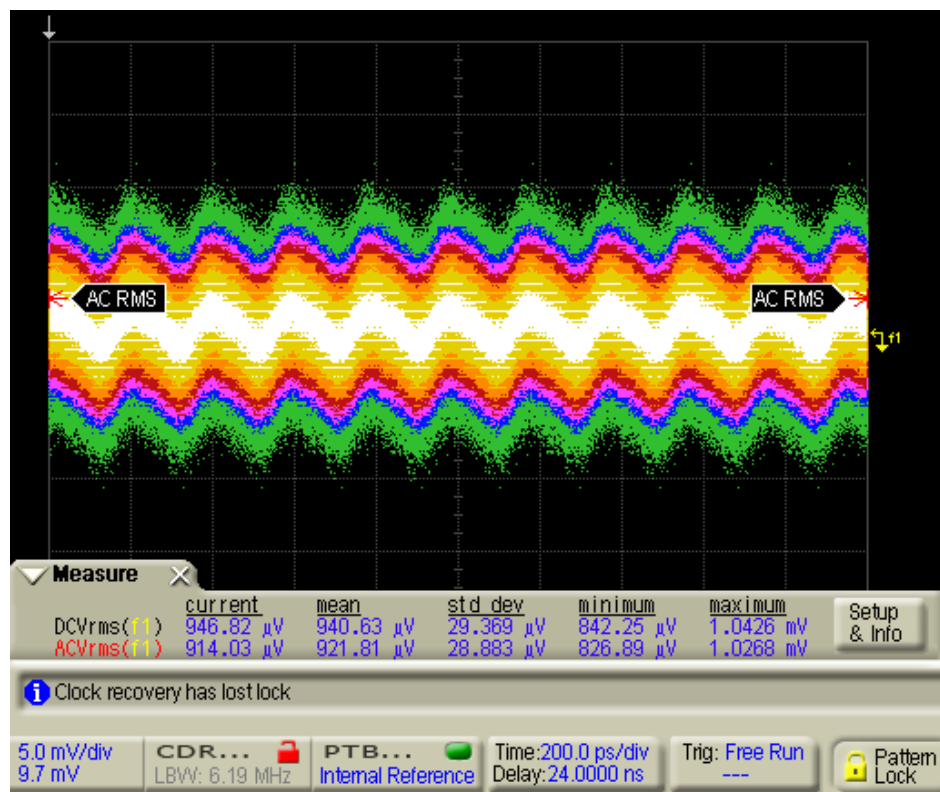


Figure 2.26. Measured NEXT RMS value is 0.9218 mV.

2.4.3. Vcm. Measurement is temporarily not available.

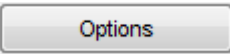
2.5. CONCLUSION

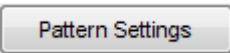
With validation of measurement, the proposed novel time domain convolution method is suitable to quantify the channel performance by calculating dWDP. It shows the advantage of less memory and time consumption compared to the frequency domain method or the traditional pulse response based convolution method.


The step response used in the proposed method can be obtained from S-parameters or directly from TDR/TDT measurement. Since VNA is considered as one of the most precise instruments in the world, the S-parameters method is more accurate than the TDR measurement. But the TDR/TDT method is potentially more useful in manufacturing floors where TDRs are commonly equipped rather than VNAs.

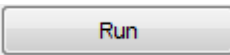
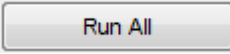
2.6. CABLE CERTIFICATION TOOL


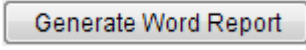
The channel performance certification algorithms were integrated into a MATLAB based “Cable Certification Tool” for calculating SFP+ copper cable parameters. In the main window of the Cable Tool, the User Name, Options, Pattern Settings can be specified. The main window is shown in Figure 2.27.

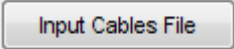
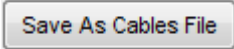
In  “Option” window, input data type, the WDPi calculation can be set (Figure 2.28).

In  “Pattern Settings” window, data pattern, tr/ta, signal amplitude, samples/bit, etc. can be set (Figure 2.29).

After the two settings above, the  “Add New Cable” button is enabled and cable under test can be added by importing S-parameters file (Figure 2.30) or step response file (Figure 2.31). A wizard for importing CSV files is shown in Figure 2.32 and a wizard for importing TXT files is shown in Figure 2.33.

Multiple cables can be added in the tool. The  “Run” button is for certification of current active cable, and the  “Run All” button is for certification of all imported cables. A report can be generated after all calculations are finished.

The  “Report” button is for generating a Matlab figure based table report for each cable added. Then a  “Generate Word Report” button is available in “Report” window for create a detailed word report (Figure 2.34).

The  “Input Cables File” button and  “Save As Cables File” button in the main window is for saving or recalling a txt file that describes the cable information. This process simplifies the cable parameter input process.

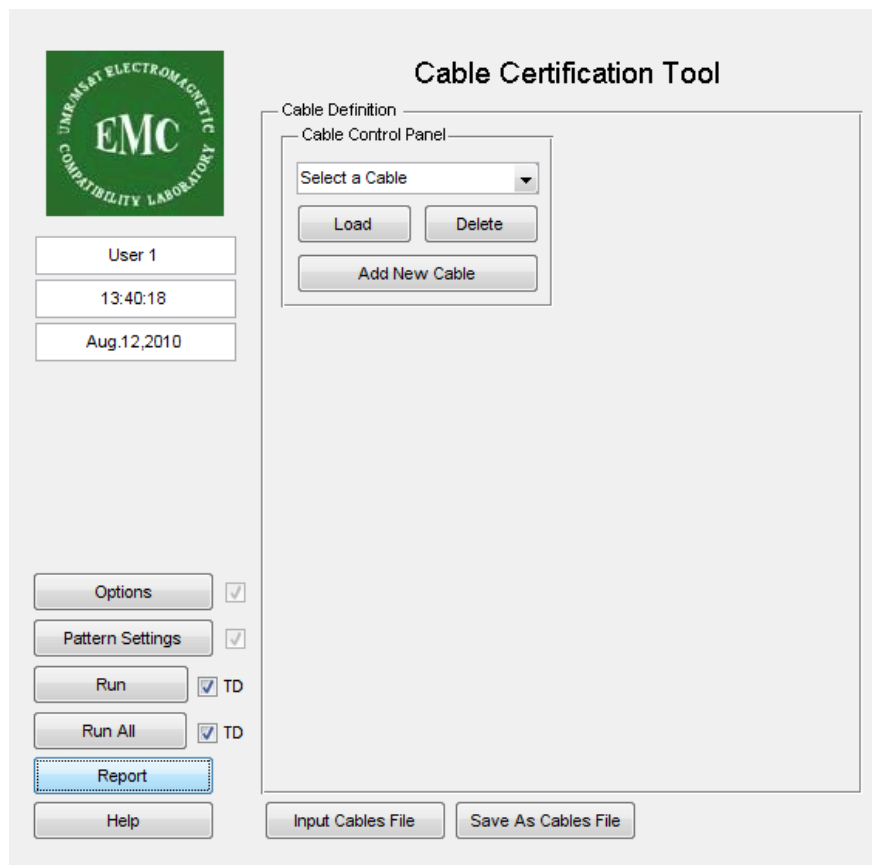


Figure 2.27. Cable certification tool main window.

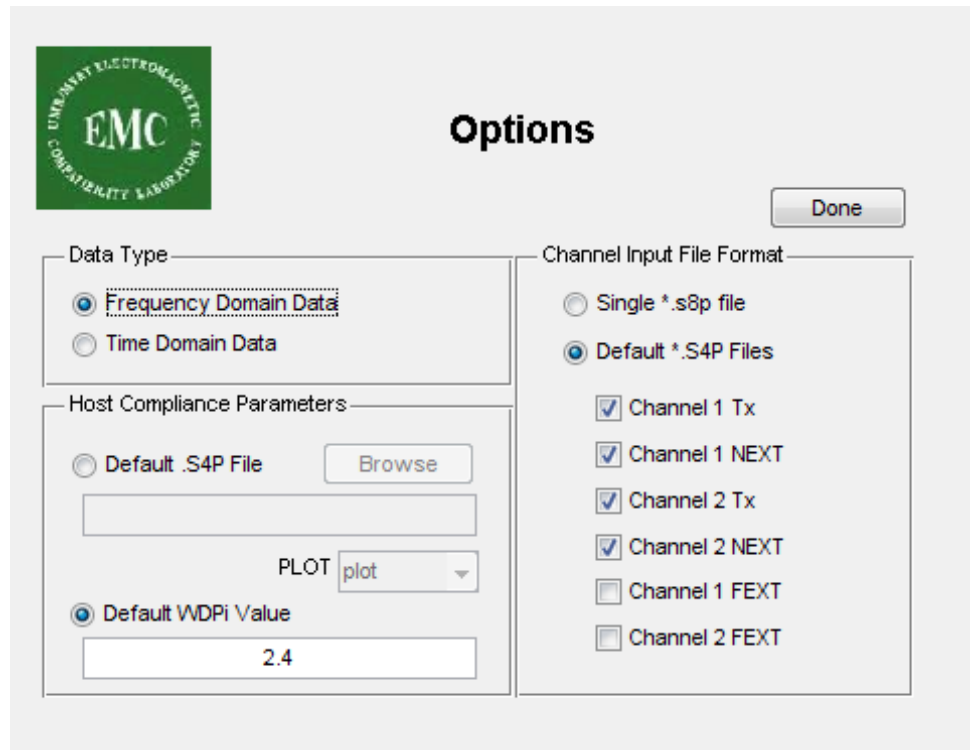


Figure 2.28. Options window for setting input data type and specify WDPi.

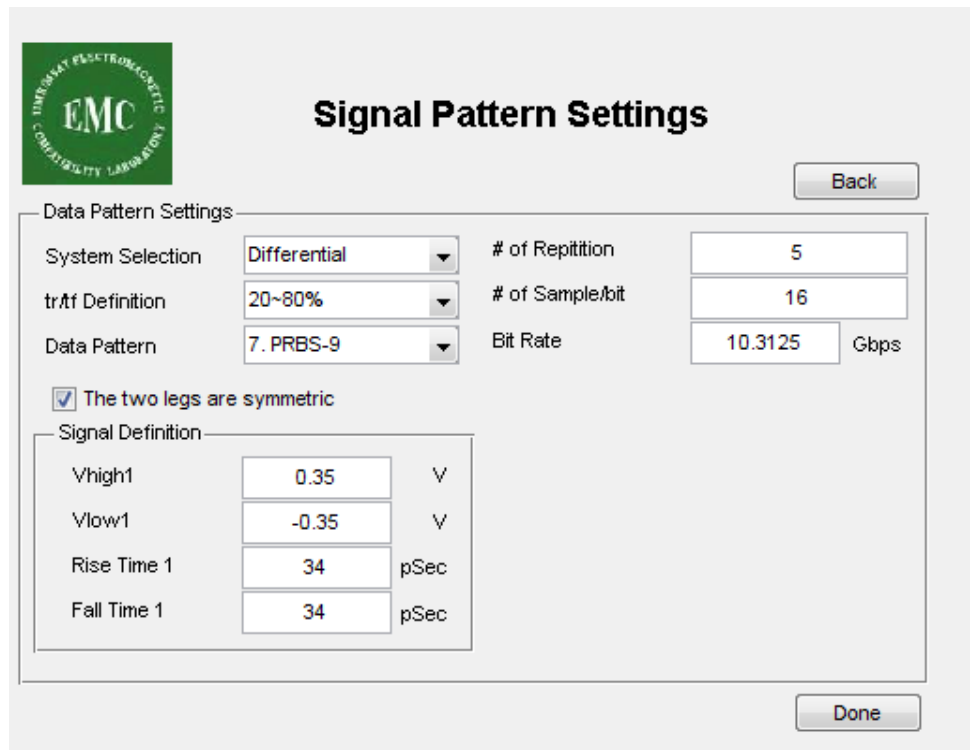


Figure 2.29. Signal pattern settings window for setting waveform parameters.

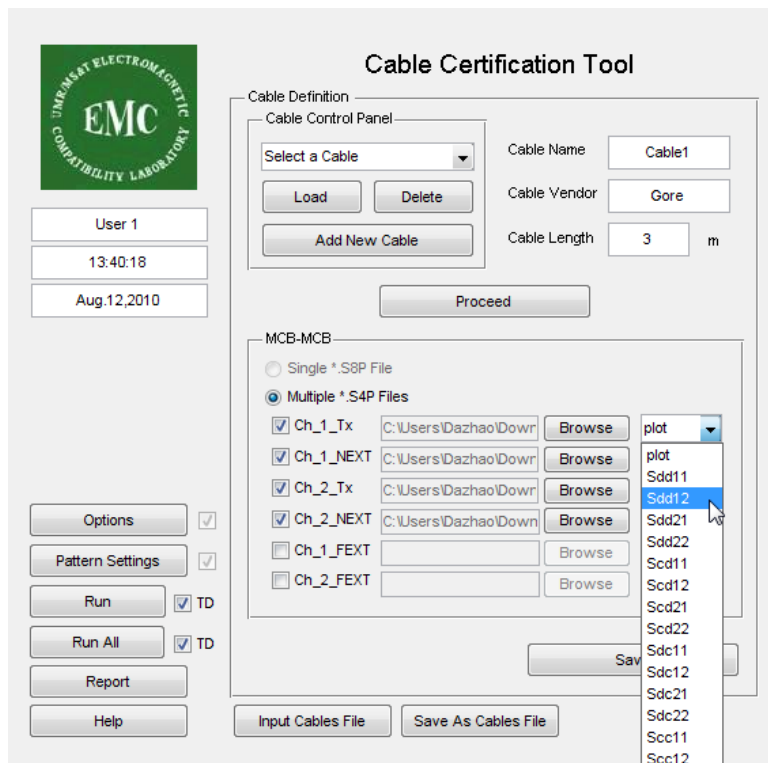


Figure 2.30. Add a new cable by importing S-parameters.

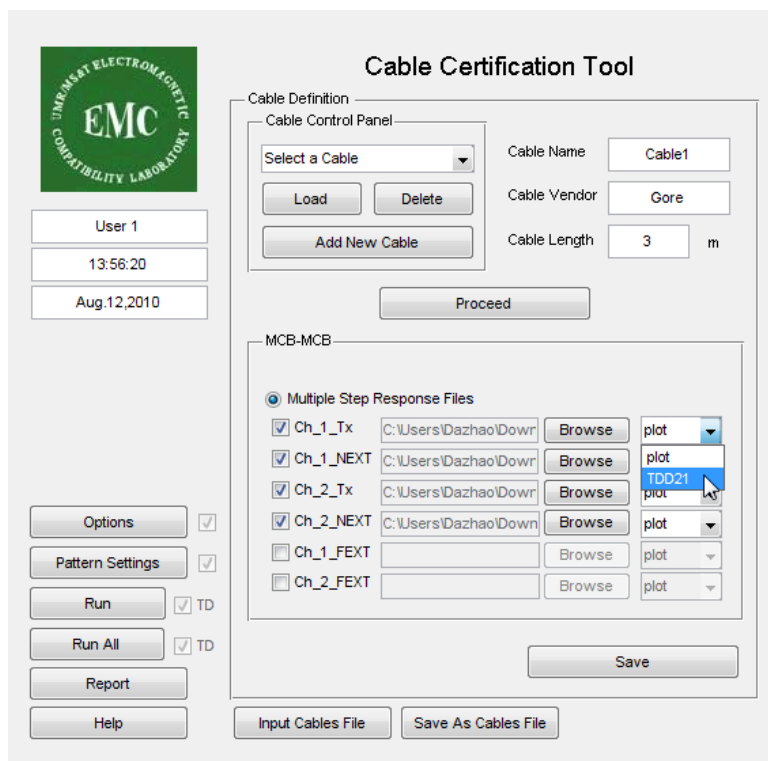


Figure 2.31. Add a new cable by importing CSV files.

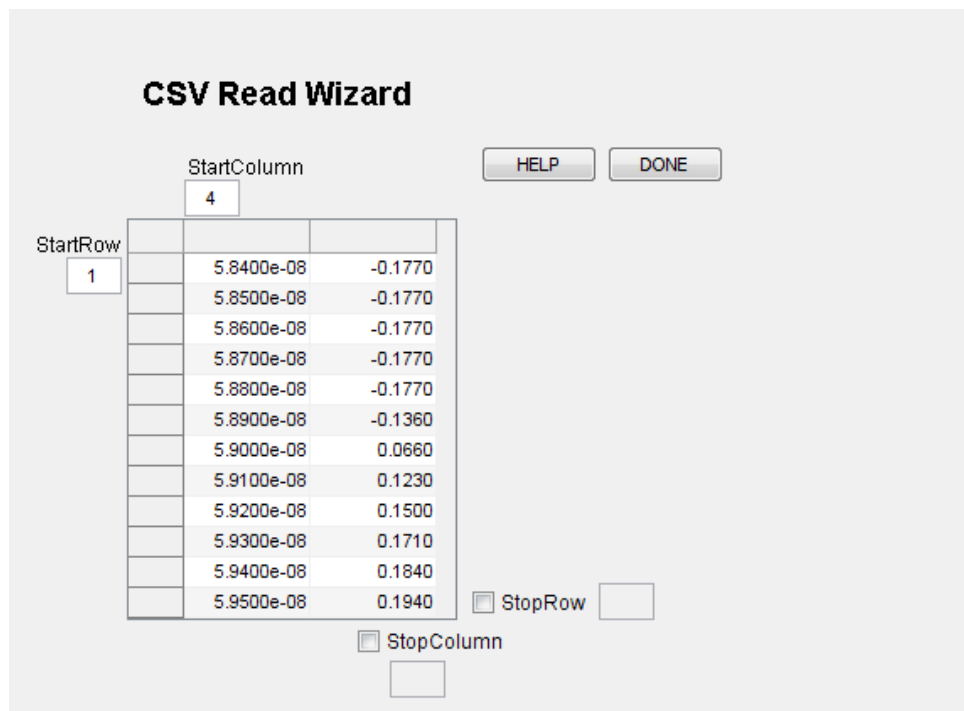


Figure 2.32. A wizard for importing CSV data files.

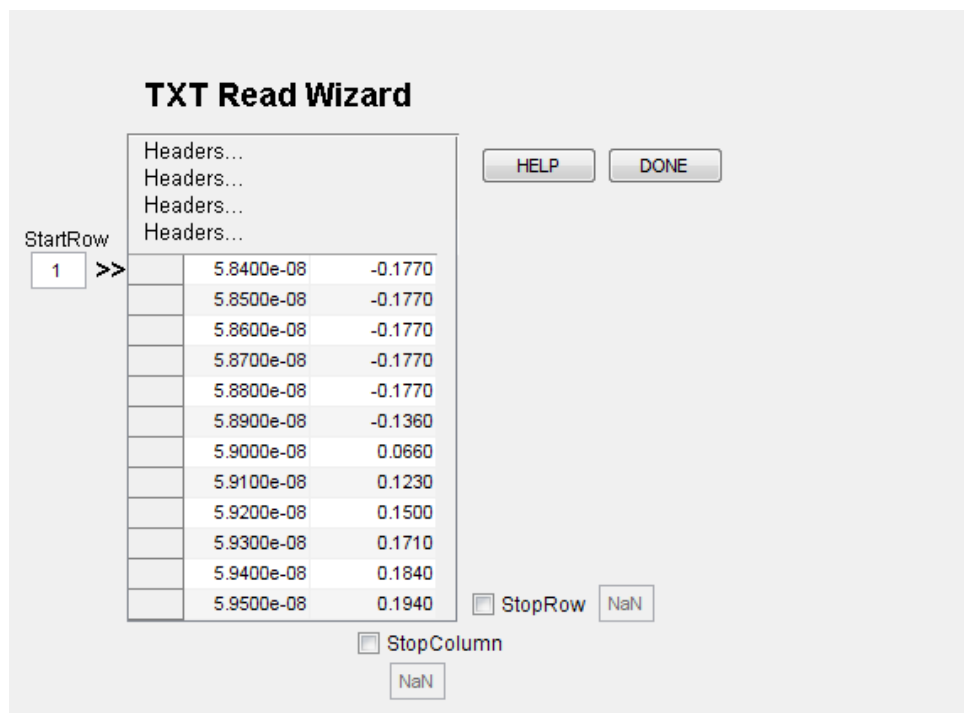


Figure 2.33. A wizard for importing TXT data files.

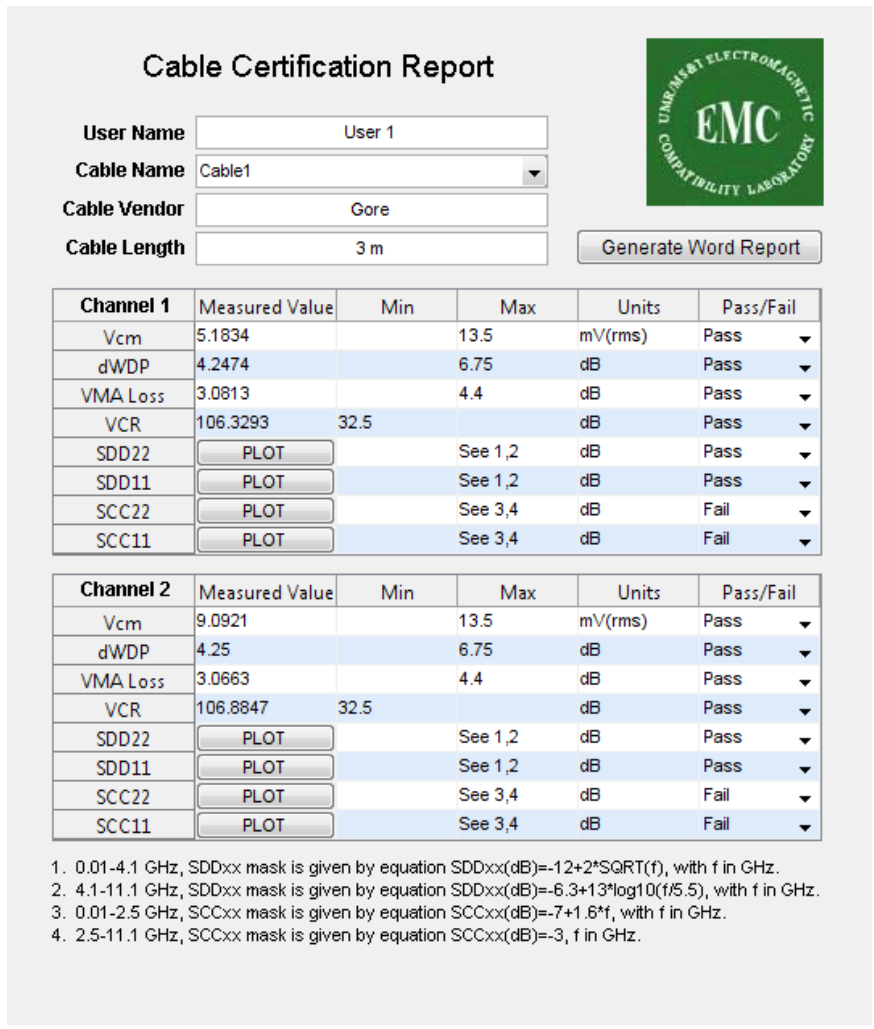


Figure 2.34. A MATLAB figure based report.

BIBLIOGRAPHY

- [1] S. Caniggia, F. Maradei, "Circuit and numerical modeling of electrostatic discharge generators," *Industry Applications, IEEE Transactions on*, vol. 42, Issue 6, Nov.-Dec. 2006. pp:1350 -1357.
- [2] G. Cerri, R. De Leo, and V. M. Primiani, "ESD indirect coupling modeling," *IEEE Trans. Electromagn. Compat.*, vol. 38, no. 3, pp. 274–281, Aug. 1996.
- [3] IEC 61000-4-2 Ed. 2.0, Electromagnetic compatibility (EMC) - Part 4-2: Testing and measurement techniques - Electrostatic discharge immunity test 2008-12-09.
- [4] J. Koo, Q. Cai, G. Muchaidze, A. Martwick, K. Wang, and D. Pommerenke, "Frequency-domain measurement method for the analysis of esd generators and coupling," *IEEE Trans, Electromagn. Compat.*, vol. 49, no. 3, pp.504-511, Aug. 2007.
- [5] H. Tanaka, O. Fujiwara, and Y. Yamanaka, "A circuit approach to simulate discharge current injected in contact with an ESD-gun," in *Proc. 3rd Int. Symp. Electromagn. Compat.* May 21–24, 2002, pp. 486–489.
- [6] K. Wang, D. Pommerenke, R. Chundru, T. V. Doren, J. L. Drewniak, and A. Shashindranath, "Numerical modeling of electrostatic discharge generators," *IEEE Trans. Electromagn. Compat.*, vol. 45, no. 2, pp. 258–271, May 2003.
- [7] F. Centola, D. Pommerenke, K. Wang, T. V. Doren, and S. Caniggia, "ESD excitation model for susceptibility study," in *Proc. IEEE Int. Symp. Electromagn. Compat.* Aug. 18–22, 2003, vol. 1, pp. 58–63.
- [8] R. Jobava, D. Pommerenke, D. Karkashadze, P. Shubitidze, R. Zaridze, S. Frei, and M. Aidam, "Computer Simulation of ESD from Voluminous Objects Compared to Transient Fields of Humans," *IEEE Trans. Electromagn. Compat.*, vol. 42, no. 1, pp. 54–65, February 2000.
- [9] Y. Taka, O. Fujiwara, "Verification of spark resistance formula for human ESD," 2008 Asia-Pacific Symposium on Electromagnetic Compatibility & 19th International Zurich Symposium on Electromagnetic Compatibility, pp. 152-155, May 2008.
- [10] R. Jobava, D. Pommerenke, D. Karkashadze, P. Shubitidze, R. Zaridze, S. Frei, R. Beria, and A. Gheonjian, "Computer simulation of ESD from cone," *DIPED-98. Proceedings of III International Seminar/Workshop on*, pp. 111-113, 1998.

- [11] R. Zaridze, D. Karkashadze, R. G. Djobava, D. Pommerenke, and M. Aidam, "Numerical calculation and measurement of transient fields from electrostatic discharges," *IEEE Trans. Components, packaging, and manufacturing technology*. Part C, vol. 19, no. 3, pp. 178-183, July 1996.
- [12] D. Pommerenke, M. Aidam, "To what extent do contact-mode and indirect ESD test methods reproduce reality," *Electrical Overstress/Electrostatic Discharge Symposium Proceedings*, 1995. 12-14 Sept. 1995, pp. 101-109.
- [13] D. Pommerenke, "ESD: transient field, arc simulation and rise time limit," *Journal of electrostatics*, ISSN 0304-3886, vol. 36, no. 1, pp. 31-54, 1995
- [14] O. Fujiwara, H. Seko, "FDTD computation modeling based on spark-resistance formula for electromagnetic fields due to electrostatic discharge", *Proc. International Wroclaw Symposium and Exhibition on Electromagnetic Compatibility*, pp.421-424, 2002.
- [15] N. Orhanovic, R. Raghuram, N. Matsui, "Full wave Analysis of planar interconnect structures using FDTD-SPICE," *Electronic Components and Technology Conference, 2001. Proceedings. 51st*, pp. 489-494, 2001.
- [16] N. Orhanovic, R. Raghuram, N. Matsui, "Nonlinear full wave time domain solutions using FDTD_SPICE for high speed digital and RF," *Wireless and Optical Broadband Conference, 2001*.
- [17] Microwave Studio, Computer Simulation Technology, [Online]. Available: <http://www.cst.com>. Date last accessed: Nov. 09th, 2010.
- [18] Meek and Craggs, "Electrical Break down of Gases," Oxford Univ. Press, Oxford, 1953 and Wiley, New York, 1978.
- [19] G. A. Mesyats, V. V. Kremnev, G. S. Korshunov and Yu. B. Yankelevich, "Spark current and voltage in nanosecond breakdown of a gas gap," *Sov. Phys. Tech. Phys.*, 14(1) (1969) 49-53.
- [20] M. Bandinu, F. Canavero, S. Grivet-Talocia, I. S. Stievano, "IdEM & M π LOG: macromodeling tools for system-level signal integrity and EMC assessment," European IBIS Summit Meeting, Apr. 19, 2007.
- [21] Broadband SPICE, Sigridy, [Online]. Available: <http://www.sigridy.com/products/bds/bds.htm>. Date last accessed: Nov. 09th, 2010.

- [22] D. L. Lin and T. L. Welsher, "From lightning to charged-device model electrostatic discharges," *ESO/ESD Symp.* (1992) 68-75.
- [23] S. Atsushi, Y. Takahiro, M. Noriaki, "Effects of the relative humidity on ESD from the charged metal," *Seidenki Gakkai Koen Ronbunshu*, vol.2006, no., pp.43-44, 2006.
- [24] Q. Cai, J. Koo, A. Nandy, D. Pommerenke, Jong Sung Lee, Byong Su Seol, "Advanced full wave ESD generator model for system level coupling simulation," *Electromagnetic Compatibility, 2008. EMC 2008. IEEE International Symposium on*, 18-22 Aug. 2008, pp. 1-6.
- [25] S. Norman L., P. Voois, T. Lindsay, and S. Zeng, "Explanation of IEEE 802.3, Clause 68 TWDP," Jan 05th, 2006, [Online]. Available: <http://ieee802.org/3/aa/public/tools/TWDP.pdf>. Date last accessed: Nov. 09th, 2010.
- [26] IEEE Std. 802.3aq-2006. 10GBASE-LRM. Published. Oct. 06th.
- [27] SFF-8431, Revision 2.1. SFP+ (Enhanced 10 Gbit pluggable module). Published. Jul. 06th, 2009.
- [28] N. Radhakrishnan, "Stressed-Eye Analysis And Jitter Separation for High-Speed Serial Links," A Thesis of Missouri University of Science And Technology, 2009.
- [29] S. Mittal, F. D. Paulis, Z. Yang, J. Fan, "Using TWDP to quantify channel performance with frequency-domain s-parameter data," *IEEE International Symposium on Electromagnetic Compatibility*, 2008.
- [30] A. Sanders, "Statistical Signal Analysis (SSA) Demystified," *EE Times-India*, August 2007.
- [31] S. Gupta, C Warwick, "Signal Integrity Design Using Fast Channel Simulator and Eye Diagram Statistics," *Agilent EEsof EDA*, July 29th, 2009.
- [32] R.S. Adve, T.K. Sarkar, "Application of the Cauchy Method for Extrapolating/Interpolating Narrow-Band System Responses," *IEEE Transactions on Microwave Theory and Techniques*, Vol. 45, NO. 5, May 1997.

- [33] S. M. Narayana, G. Rao, R. Adve “Interpolation/Extrapolation of Frequency Domain Responses Using the Hilbert Transform,” IEEE Transactions on Microwave Theory and Techniques, Vol. 44, NO. 10, October 1996.
- [34] H. Shi, “A Refinement Procedure for S-Parameter DC Extrapolation based on Sampling Theorem and Causality,” Electrical Performance of Electronic Packaging, 2007.
- [35] X. Gao, Q. Chen, “Comparisons of different S parameter DC extrapolation methods and their impacts on equalization,” Intel Corporation.
- [36] P. Triverio, S. G. Talocia, “Robust Causality Characterization via Generalized Dispersion Relations,” IEEE Transactions on Advanced Packaging, Vol. 31, NO. 3, August 2008.
- [37] B. Gustavsen, A. Semlyen, “Rational Approximation of Frequency Domain Responses by Vector Fitting,” IEEE Transactions on Power Delivery, Vol. 14, NO. 3, July 1999.
- [38] A. Chinae, P. Triverio, and S. Grivet-Talocia, “Delay-based macromodeling of long interconnects from frequency-domain terminal responses,” IEEE Trans. Adv. Packag., to be published.
- [39] A. Chinae, P. Triverio, and S. Grivet-Talocia, “Compact macromodeling of electrically long interconnects,” in Proc. 17th Top. Elect. Perform. Electron. Packag. Meeting, San Jose, CA, Oct. 2008, pp. 199–202.
- [40] S. Grivet-Talocia, “Delay-based macromodels for long interconnects via time-frequency decompositions,” in Proc. IEEE 15th Elec. Perform. Electron. Packag., Top. Meeting, Scottsdale, AZ, Oct. 2006, pp. 199–202.
- [41] R. Mandrekar and M. Swaminathan, “Causality enforcement in transient simulation of passive networks through delay extraction,” in 9th IEEE Signal Propag. Interconnects Workshop, Garmisch-Partenkirchen, Germany, May 10–13, 2005, pp. 25–28.
- [42] R. Mandrekar and M. Swaminathan. “Delay extraction from frequency domain data for causal macro-modeling of passive networks,” In Proc. Int. Symp. Circuits and Systems, Volume 6, pages 5758–5761, May 2005.
- [43] P. A. Perry, T. J. Brazil, “Hilbert-Transform-Derived Relative Group Delay,” IEEE Transactions On Microwave Theory And Techniques, Vol. 45, No. 8, August 1997.

- [44] B. Gustavsen, "Time delay identification for transmission line modeling," in 8th IEEE Signal Propag. Interconnects Workshop, Hildesheim, Germany, May 2004, pp. 103–106.
- [45] N. M. Nakhla, A. Dounavis, R. Achar, and M. S. Nakhla, "DEPACT: Delay extraction-based passive compact transmission-line macro-modeling algorithm," IEEE Trans. Adv. Packag., vol. 28, no. 2, pp. 13–23, Feb. 2005.
- [46] A. Oppenheim, R. Schaffer, "Discrete-time Signal Processing," 2nd ed. Prentice Hall, 1999, Ch 5.1 I.
- [47] P. A. Perry, T. J. Brazil, "Forcing Causality on S-Parameter Data Using the Hilbert Transform," IEEE Microwave and Guided Wave Letters, Vol. 8, No. 11, November 1998.
- [48] F. Rao, C. Morgan, S. Gupta, V. Borich, "The Need for Impulse Response Models and an Accurate Method for Impulse Generation from Band-Limited S-Parameters," DesignCon 2008.
- [49] F. Rao, "Optimization of Spectrum Extrapolation for Causal Impulse Response Calculation Using the Hilbert Transform," US Patent, Pub. No.: US2008/0281893 A1.
- [50] H. M. Nussenzveig, Causality and Dispersion Relations. New York: Academic, 1972.
- [51] E. J. Beltrami and M. Wohlers, Distributions and the Boundary Value of Analytic Functions. New York: Academic, 1966.
- [52] P. Triverio and S. Grivet-Talocia, "A robust causality verification tool for tabulated frequency data," presented at the 10th IEEE Workshop Signal Propagation Interconnects, Berlin, Germany, May 9–12, 2006.
- [53] P. Triverio and S. Grivet-Talocia, "On checking causality of band-limited sampled frequency responses," in 2nd Conf. Ph.D. Res. Microelectron. Electron. (PRIME), Otranto, Italy, Jun. 12-15, 2006, pp. 501–504.
- [54] P. Triverio and S. Grivet-Talocia, "Robust causality characterization via generalized dispersion relations," IEEE Trans. Adv. Packag., vol. 31, no. 3, pp. 579–593, Aug. 2008.

- [55] Wikipedia, http://en.wikipedia.org/wiki/Central_limit_theorem. Date last accessed: Nov. 09th, 2010.
- [56] Wikipedia, http://en.wikipedia.org/wiki/Cauchy-Schwarz_inequality. Date last accessed: Nov. 09th, 2010.
- [57] J.H. Lee, H.T. Kim, "Natural Frequency Extraction Using Generalized Pencil-Of-Function Method And Transient Response Reconstruction," Progress In Electromagnetics Research C, Vol. 4, 65–84, 2008.
- [58] Y. Hua, T. K. Sarkar, "Generalized Pencil-of-Function Method for Extracting Poles of an EM System from Its Transient Response", IEEE Trans on Antennas and Propagation, Vol. 37, No. 2, February, 1989.
- [59] S. Pannala, "Development of Time Domain Characterization Methods for Packaging Structures", a Ph. D Dissertation, Georgia Institute of Technology, August, 1999.
- [60] S. Pannala, M. Swaminathan, "Extraction of S-Parameters from TDR/TDT Measurements using Rational Functions", 54th ARFTG Conf. Dig., pp 45-52, Fall 1999.

VITA

Dazhao Liu was born on March 13th, 1986 in Qingyang City, Gansu Province, P.R. China. In May 2008, he received his Bachelor of Science, Electrical Engineering in Electrical Engineering Department of Tsinghua University, Beijing, P. R. China.

In August 2008, he enrolled at the Missouri University of Science and Technology to pursue his Master's Degree in Electrical Engineering, since when, he was a graduate research assistant in Electromagnetic Compatibility Laboratory.